

ANALYSIS OF INDIVIDUAL, COMBINED AND 2-STEP VARIATION IN
INDUCTION SYSTEM OF AN IC ENGINE TO OPTIMIZE PERFORMANCE AND
FUEL EFFICIENCY

by

Pauras Sawant

A thesis submitted to the faculty of
The University of North Carolina at Charlotte
in partial fulfillment of the requirements
for the degree of Master of Science in
Mechanical Engineering

Charlotte

2018

Approved by:

Dr. Saiful Bari

Dr. Mesbah Uddin

Dr. Peter Tkacik

ABSTRACT

PAURAS SAWANT, Analysis of individual, combined and 2-step variation in the induction system of an IC engine to optimize performance and fuel efficiency
(Under the guidance of DR. SAIFUL BARI)

Naturally aspirated internal combustion (IC) engines with conventional intake assembly are tuned only over a narrow speed range to produce an induction boost by capitalizing the pressure waves arising in the intake manifold. In this research, intake runner length, intake valve timing, and intake valve lift, being key contributors to the wave and in-cylinder gas dynamics, are varied individually and simultaneously over a range of values to capitalize the induction pressure waves to boost the engine volumetric efficiency and thus the overall performance and fuel efficiency at all operating speeds. The engine studied is a single-cylinder, four-stroke, spark-ignited, 510 cc, gasoline engine. The 1-D model of the stock engine built in Ricardo Wave software is validated with 98 % accuracy against experimental test results to simulate engine's stock performance at wide open throttle (WOT). Infinite variations in individual parameters can optimize engine performance but are not feasible due to assembly and space constraints. Simultaneous variations of parameters reduce the number and the span of variations required to optimize engine performance. To further simplify the assembly, two values of each of the above-mentioned parameters giving optimal performance are chosen. As a result, 5.96 percent increment in engine performance is encountered but at the cost of 0.24 percent rise in brake specific fuel consumption (BSFC). To reduce BSFC, the air-fuel ratio is varied as per the load and speed requirements to match stock engine performance. Running the engine on comparatively leaner air-fuel mixtures reduces BSFC by an average of 3.9 percent as compared to stock engine fuel efficiency.

ACKNOWLEDGEMENTS

Foremost, I would like to express my sincere gratitude and indebtedness to my mentor and advisor Dr. Saiful Bari for giving me this opportunity to work on a topic of my immense interest. He has been a constant source of guidance, inspiration, motivation and immense knowledge. I would also like to thank him for keeping faith in me, being patient and letting me explore my ideas independently.

I would also like to express my sincere gratitude to the thesis committee members Dr. Mesbah Uddin, Dr. Peter Tkacik and all the faculty and staff of the motorsports research laboratory. I would also like to thank the mechanical engineering department of UNCC for providing me all the necessary resources to complete this thesis. The validation of the model that the thesis is based on would not have been possible without the engine test data provided by the UNCC Formula Student (FSAE) team of 2017. I am very thankful for their help and support.

A special thanks to my seniors, my fellow lab mates and classmates in UNCC for their support, for the stimulating discussions we have had, for accompanying me through the spending sleepless nights to meet deadlines and for making this a fun-filled and memorable journey.

Last but not the least, I would like to thank my parents Vinay Sawant and Vrushali Sawant for supporting my every endeavor in life, for helping me rise when I am fail and teaching me to keep me to stick to the ground and be humble when I succeed.

TABLE OF CONTENTS

LIST OF TABLES	vii
LIST OF FIGURES	viii
1: INTRODUCTION	1
1.1: BACKGROUND	1
1.2: ENGINE TUNING	4
1.3: CHALLENGES WITH CONVENTIONAL ENGINE TUNING	7
1.4: VARIABLE INDUCTION SYSTEMS	8
1.5: RECENT ADVANCEMENT IN VARIABLE INDUCTION SYSTEMS	11
2: METHODOLOGY	12
2.1: CHRYSLER'S RAM AIR THEORY	12
2.2: PRESSURE WAVE CAUSES	13
2.3: PRESSURE WAVE SPEED	14
2.5: ENGELMANN'S FORMULA	18
2.6: EFFECTS OF INTAKE VALVE OPEN AND CLOSING TIMINGS	19
2.7: ENGINE SELECTION	21
2.8: 1-D SIMULATION MODEL	23
2.9: VALIDATION OF THE MODEL	34
2.10: CASE SET-UP FOR FURTHER SIMULATIONS	42
3: RESULTS AND DISCUSSION	46
3.1: EFFECTS OF VARYING RUNNER LENGTHS	47
3.2: EFFECTS OF VARYING INTAKE VALVE TIMING	52
3.3: EFFECTS OF VARIABLE INTAKE VALVE LIFT	57

3.4: INDUCTION PRESSURE WAVES	63
3.5: EFFECTS ON POWER AND TORQUE PERFORMANCE	67
3.6: EFFECTS ON SPECIFIC FUEL CONSUMPTION	71
3.5: VARIATIONS IN AIR-FUEL RATIO	73
4: CONCLUSIONS	79
5: REFERENCES	82

LIST OF TABLES

TABLE 1: Engine Specifications	22
TABLE 2: Dominant input parameters used for uncertainty evaluation	37
TABLE 3: Combine standard uncertainty of simulated power at each engine speed	39
TABLE 4: Volumetric efficiency variations with respect to (wrt) runner lengths	51
TABLE 5: Comparison of volumetric efficiency wrt variable valve timings	56
TABLE 6: Comparison of volumetric efficiency wrt variable valve lifts	61

LIST OF FIGURES

FIGURE 1: Typical Histogram of Engine Speed (rpm) vs Throttle angle (%)	3
FIGURE 2: Acoustic Resonance	10
FIGURE 3. Conventional valve timing diagram	10
FIGURE 4: Pressure wave along intake runner	13
FIGURE 5: Plenum and Intake runner layout	15
FIGURE 6: Plenum and intake runner diagram	16
FIGURE 7: Ricardo WaveBuild Window at startup	24
FIGURE 8: Simulation Control Tab	25
FIGURE 9: 2-D model of the engine	26
FIGURE 10: Cylinder Panel	29
FIGURE 11: Chen-Flynn friction correlation coefficients	30
FIGURE 12: SI Wiebe combustion submodel	31
FIGURE 13: Intake valve profile	33
FIGURE 14: Exhaust valve profile	33
FIGURE 15: Brake power v/s engine speed - Simulation results validated against experimental power	34
FIGURE 16: Brake torque v/s engine speed - Simulation results validated against experimental power	35
FIGURE 17: Normal probability distribution plots at each engine speed simulated (rpm)	38
FIGURE 18: Engine power histogram for each engine speed	39

FIGURE 19. Comparison of simulated and experimentally measured engine power (coverage factor = 1)	40
FIGURE 20. Comparison of simulated and experimentally measured engine power (coverage factor = 2).	40
FIGURE 21: Simulated runner lengths	42
FIGURE 22. Simulated valve opening time range	44
FIGURE 23. Simulated valve lift range	45
FIGURE 24: Variations in volumetric efficiency with respect to intake runner lengths	46
FIGURE 25: Best intake runner lengths for each engine speed	48
FIGURE 26: Peak volumetric efficiency with multiple variations in runner lengths	48
FIGURE 27: Two best runner lengths to optimize volumetric efficiency	50
FIGURE 28: Comparison of volumetric efficiency (i) original runner length, (ii) infinitely variable runner lengths (iii) two runner lengths	50
FIGURE 29: Variations in volumetric efficiency with respect to (wrt) intake valve opening timing	52
FIGURE 30: Best valve opening times for each engine speed	53
FIGURE 31: Peak volumetric efficiency with 2 variations in runner length and multiple variations in valve timing	53
FIGURE 32: Two best valve opening timings along for optimized volumetric efficiency	55

FIGURE 33: Comparison of volumetric efficiency- (i) original, (ii) 2 runner lengths + variable valve timings, (iii) 2 runner lengths + 2 valve opening timings	55
FIGURE 34: Volumetric efficiency variations with respect to (wrt) variable intake lift multipliers	57
FIGURE 35: Best valve lift multipliers for each engine speed.	59
FIGURE 36: Peak volumetric efficiency with 2 variations in runner lengths and valve timings and multiple variations in valve lifts	59
FIGURE 37: Two best valve opening timings along for optimized volumetric efficiency	60
FIGURE 38: Comparison of volumetric efficiency- (i) original, (ii) 2 runner lengths + 2 valve timings + variable valve lifts, (iii) 2 runner lengths + 2 valve opening timings + 2 valve lifts	60
FIGURE 39: Comparison of valve profile and pressure waves for the case with original intake assembly at 6000 rpm	64
FIGURE 40: Comparison of valve profile and pressure waves for the case with 2 variations in runner lengths at 6000 rpm	64
FIGURE 41: Comparison of valve profile and pressure waves for the case with original intake assembly at 6000 rpm	65
FIGURE 42: Comparison of valve profile and pressure waves for the case with original intake assembly at 6000 rpm	65
FIGURE 43: Comparison of in-cylinder pressures for 6000 rpm	67
FIGURE 44: Comparison of pressure volume diagrams for 6000 rpm	67
FIGURE 45: Comparison of maximum achievable brake power	69

FIGURE 46: Comparison of maximum achievable brake torque	69
FIGURE 47: Comparison of maximum achievable brake torque	70
FIGURE 48: Comparison of thermal efficiency for various cases	71
FIGURE 49: Comparison of thermal efficiency for various cases	71
FIGURE 50: Comparison of thermal efficiency for various cases	72
FIGURE 51: Air-Fuel ratios to match stock engine performance	73
FIGURE 52: Comparison of pressure-volume diagram at 6000 rpm	74
FIGURE 53: Comparison of temperature-entropy diagram at 6000 rpm	75
FIGURE 54: Comparison of thermal efficiency	77
FIGURE 55: Comparison of BSFC	77
FIGURE 56: Percentage improvement in fuel efficiency	78

1: INTRODUCTION

1.1: BACKGROUND

The current day advancements in the field of IC engines can be broadly classified into two types. The first type aims at increasing the engine performance (torque and power) at the cost of increased fuel consumption. Whereas, the second type of advancements aim at increasing the fuel efficiency at the cost of engine performance [1]. Extensive research is going on in the field of induction systems for ICE. For an engine with a fixed air induction assembly, the tradeoff between engine torque and fuel efficiency is difficult. If the engine performance increases, the fuel efficiency decreases and vice-versa [2].

Keeping in mind the consumer's demand of increased performance and the Environmental Pollution Agency's (EPA) [3] requirements of increased fuel efficiency, this research aims at blending the above two types and providing the consumer an engine that will satisfy his need of increased performance when driving on race tracks and save money and fuel with increased fuel efficiency when driving on highway or interstate roads.

Engine, the only power producing device in a vehicle is a very vital component, affecting the overall performance of a road vehicle. Internal combustion engines, however, unlike electric motors do not produce constant power throughout its operating speed range. For automotive applications, the operating speed of the engine needs to be varied as per the loading conditions, which is a function of the desired speed and torque required to produce the corresponding vehicle acceleration.

The desired vehicle and torque are subject to change continuously throughout the duration of its operation with respect to throttle angle as can be seen in the Figure (1) [4], vehicle velocity and desired acceleration of the vehicle. When the vehicle is running, a

single set of parameters will not be enough to optimize the performance of an internal combustion engine at all operating engine speeds. This problem can be resolved in two ways. First, by designing an infinitely variable transmission that would allow the engine to operate at a single operating speed where peak performance is attained, and the transmission can vary the desired speed and torque as per the load conditions. However, due to its belt driven orientation, low transmission efficiency, and inability to transfer high torque at low engine speeds, the application of infinitely variable transmission until lately has been limited only to smaller automobiles. This approach also has issues with reliability, weight and packaging [5]. The second approach is by varying a set of parameters which governs the overall performance of the engine at different operating speeds to run the engine optimally. The second option, which is more feasible, attainable, reliable and comparatively easy to package is being explored widely in the automotive and motorsports industries and this research would be contributing to the same [2, 6-8].

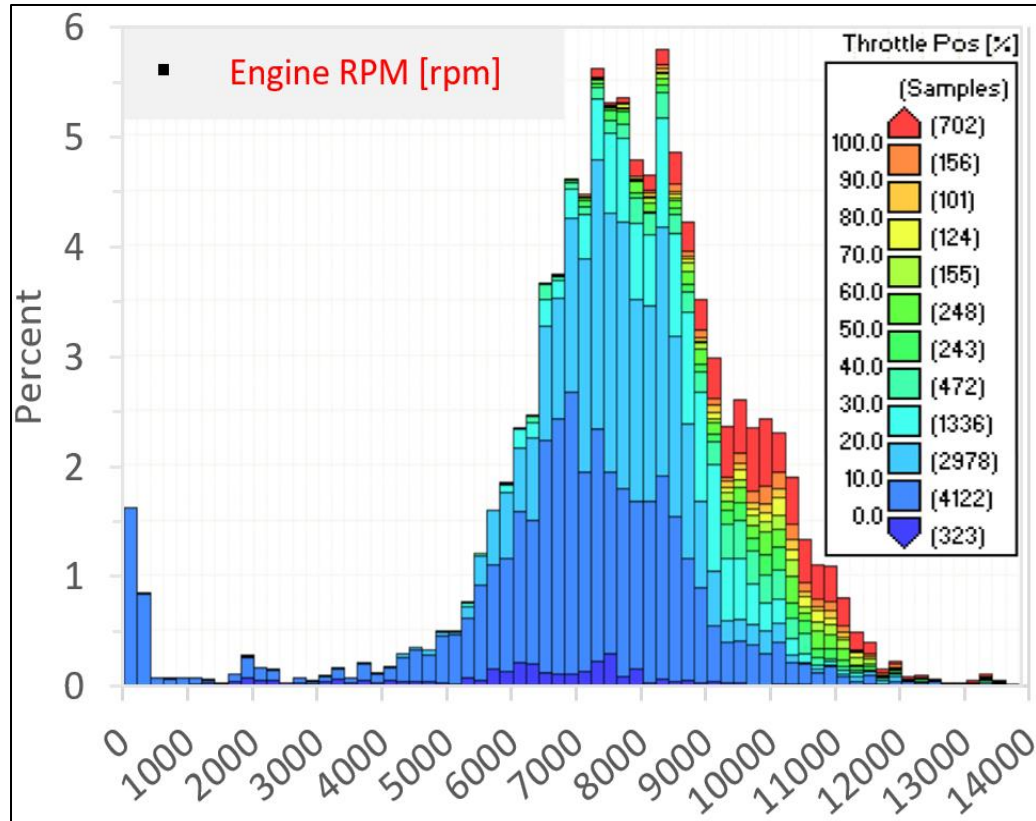


FIGURE 1: Typical Histogram of Engine Speed (rpm) vs Throttle angle(%) [4]

1.2: ENGINE TUNING

Over the past 130 years massive improvements in the field of engines have been made [2, 4-15]. Optimization of automotive engine is the most challenging task due to the operation of the engine over a wide range of engine speeds and load conditions. Engine breathing along with combustion chamber design governs the gas dynamics in the cylinder and is also a major contributor to the engine's performance. It involves inhaling fresh air/charge inside the combustion chamber and expelling the burnt gases out of combustion chamber [9]. This process is complex and depends on multiple design parameters such as port volume, port diameter, port length, port taper, valve size, number of valves, valve timing and lift [1, 4, 13, 15-17]. Optimum gas exchange process calls for balanced design of the above-mentioned parameters. Hence for efficient performance across the range of engine speeds, design of induction and exhaust systems assemblies must be optimized. This challenge has led to various arrangements for improving these gas exchange processes. One of the approaches is tuning intake port lengths which plays a significant role in providing an extra boost to the induction pressure. This pressure boost would increase the volumetric efficiency of the engine [9].

Volumetric efficiency may be defined as the measure of mass of air inducted into the cylinder as a ratio of the mass of air that can be contained in the cylinder volume [18]. In equation form:

$$\eta_v = \frac{m_g}{m_{tn}} = \frac{v_a * \rho_{th}}{V_{th} * \rho_{th}} = \frac{v_a}{v_{th}} \quad (1)$$

Where,

η_v -Volumetric efficiency

m_g -Actual mass of air inducted

m_{th} -Theoretical mass of air that can be contained in cylinder

ρ_{th} -Density of ambient air

v_a -Volume of air inducted

v_{th} -Swept volume

Sound waves are generated due to the engine suction pressure during the intake stroke, pressure differential between exhaust port and intake port during the valve overlap period and most dominant ones are produced due to valve closing events [19]. The reasons for their occurrence and their nature has been discussed in greater details in section 3.1. These sound waves have energy, tone and amplitude which go on increasing as they travel back and forth as undulating pulsations in the intake runners and exhaust headers [20]. The idea of wave tuning an engine is to increase induction boost by capitalizing the high-pressure compression wave waves in the intake runners and scavenging efficiently by capitalizing the low-pressure rarefaction wave in the exhaust headers [6, 7].

Hence, engine tuning can be defined as the selection of appropriate parameters affecting engine's breathing capacity/efficiency to capitalize these compression and rarefaction pressure waves generated in the intake and exhaust systems for getting a boost in inducting fresh charge into the combustion chamber and scavenging the exhaust gases out of the combustion chamber, thus improving volumetric efficiency. When these induction pressure waves are captured the static pressure differential between the air above the intake valve and vacuum in the cylinder (below the intake valve) increases [21]. This increases the amount of air being inducted during the suction stroke and exhaled in the exhaust stroke, thereby increasing the volumetric efficiency as is evident from Equation

(1). With the increase in the mass of air inducted, the oxygen molecules available for combustion of injected fuel increase. This will lead to complete combustion of fuel leading to increase in fuel efficiency and will also reduce the CO emission. Now with the excess amount of air available at part-load conditions, peak cycle temperature will be lowered and causing a reduction in NO_x emissions [10, 22]. Hence boosting the volumetric efficiency will increase power, torque and at the same time also increase fuel efficiency and reduce emissions [23].

1.3: CHALLENGES WITH CONVENTIONAL ENGINE TUNING

The location of the power band along the engine speed range is a major topic of discussions when race engine builders talk about 'parts integration'. The engine air induction system can be "tuned" or designed intentionally to have features which can improve the way the cylinder fills and determine the location of the peak torque along the rpm range. This is what we call intentional "power band location" placement [24]. The induction systems, with fixed dimensions, generally tuned for a single engine operating speed, will help to boost the performance of the vehicle at that speed. However, as much as tuning helps to increase the performance at the speed the engine is tuned for, it may also hurt the performance of the engine at other speeds. This hurdle has deterred the engine designers to design engines to work at their optimum capacity over its operating range for years [2, 8].

This problem is conventionally addressed in two ways, for race cars and passenger vehicles. First, by increasing the performance at a single engine speed at the cost of performance at other engine speeds. In race cars, engines are tuned to produce peak performance for a single engine speed at the cost of performance at other speed and drivers are instructed to operate around that engine speed as much as possible. The second way to address this problem is to compromise on peak power for getting a flat power curve. In the case of passenger vehicles, the drivers are not so skilled and might not be able to operate the engine just at around a single engine speed. So, the engines are tuned to produce decent performance over a range of engine speed at the cost of peak performance at a particular speed [9, 15].

1.4: VARIABLE INDUCTION SYSTEMS

The need of peak performance like a race car and the flexibility of attaining it over a range of engine speed like passenger vehicles, creates the need for variable intake systems. A comparative study on the effects of tuning for induction of fresh charge versus effects of tuning for scavenging of exhaust gas suggests that intake tuning can boost the performance of an IC engine by over 12% as compared to exhaust tuning which could increase the performance by 5%. It also suggests that tuning intake manifold and exhaust manifold are mutually independent and the effect of tuning both ends would result in an improvement which is the sum of the contribution of them both [13]. As mentioned before, this research focuses on the part contributing most to the volumetric efficiency and power/torque output i.e. the intake tuning [2, 6-8].

As discussed earlier, tuning intake systems involves creating an induction pressure boost when the intake valve opens. Sammut et al. [13] a proposed reflective wave theory for tuning of intake length at a particular engine speed to maximize volumetric efficiency, suggesting that intake tuning depends primarily on piston motion and resonance characteristics of the intake air as can be seen in Figure 2 [24, 25]. The major reasons for the occurrences of the pressure waves and their nature has been discussed in section 2.2. As these waves depend mainly on engine speed, researchers try to optimize runner length for the operating range of engine speeds. The optimal runner lengths producing peak performance for a particular engine speed are functions of valve opening and valve closing events [9, 13, 14]. So, varying valve timing with respect to engine speed can not only reduce the required variations in the runner lengths but can also further boost the performance of the engine. The coefficient of flow, kinetic energy and turbulence intensity

of the air flowing through the intake valve are strongly dependent on the cross-section area available for the intake air to flow in to the combustion chamber. The area of flow is determined by the valve diameter and the valve lift. Varying valve lifts according to the engine speed will grant a precise control of the pressure wave and help to boost the volumetric efficiency, torque and thus, fuel efficiency at all engine speeds [9, 10, 26].

Figure 3 [27] shows a conventional valve time diagram which has a fixed valve opening and closing time for all engine speeds. The intake runner lengths and valve lifts are fixed for all engine operating speeds in a conventional engines induction assembly. They are usually designed to give balanced performance at all engine speeds rather than being biased to any single engine speed. However, the ideal situation would be to create an induction boost across the engine's entire operating speed range. This would require an infinitely variable port and valve geometries [15]. This challenge has led the engine manufacturers to explore the possibilities of varying the geometry of multiple components of the engine induction assembly.

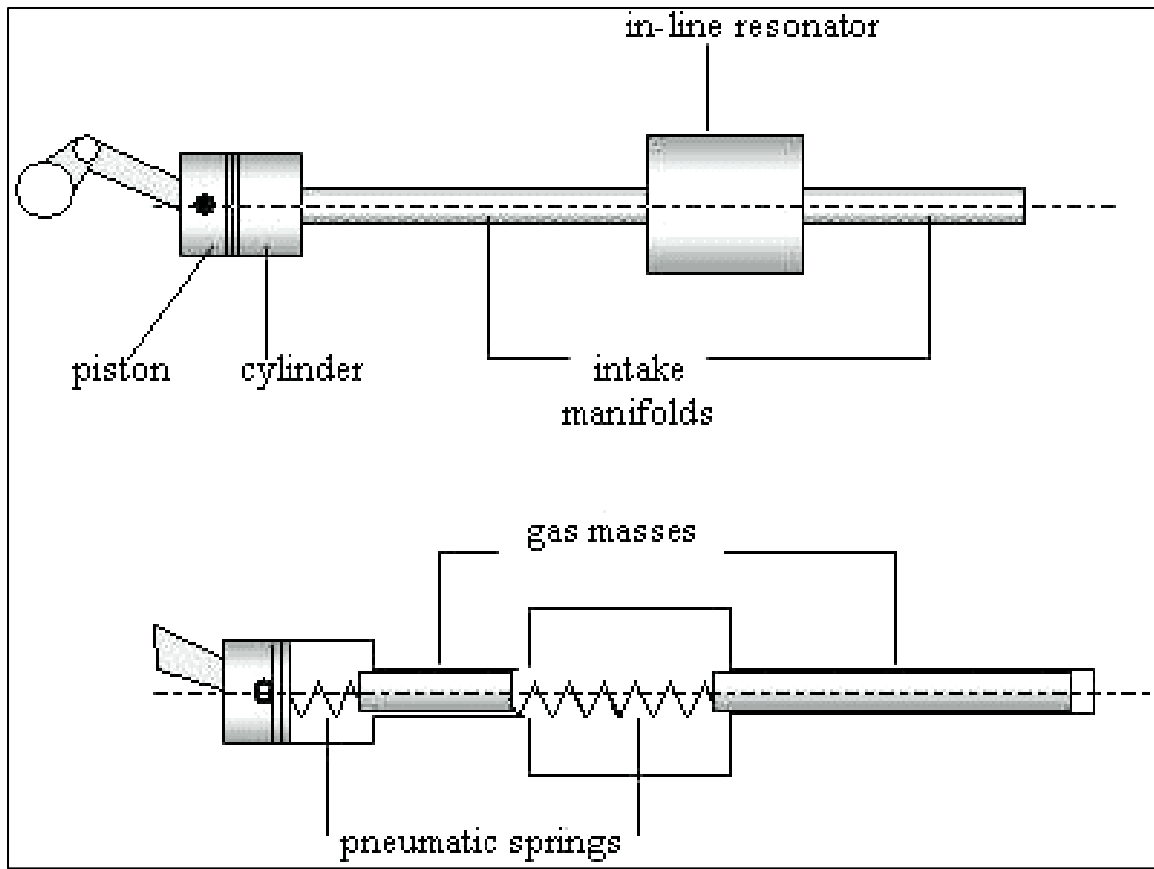


FIGURE 2: Acoustic Resonance [24, 25]

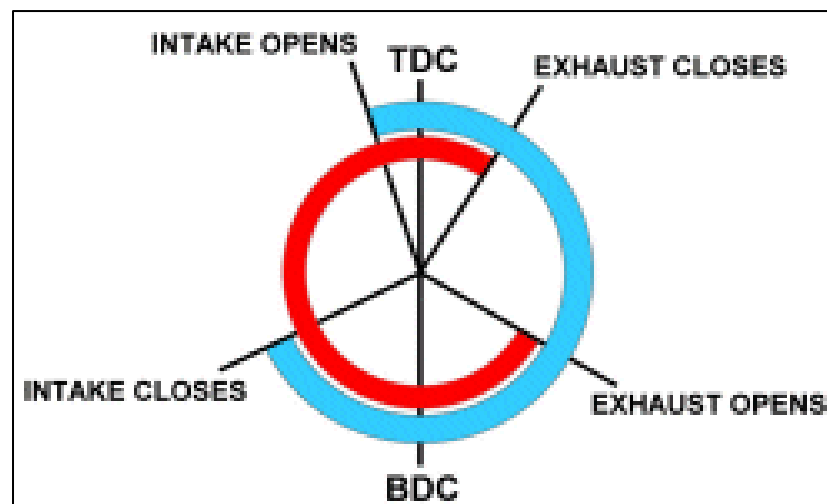


FIGURE 3. Conventional valve timing diagram [27]

1.5: RECENT ADVANCEMENT IN VARIABLE INDUCTION SYSTEMS

A few of the possibilities explored are variable runner lengths, variable runner diameter, variable plenum volume, variable valve lifts, variable valve timings and profile. Varying the runner diameters, lengths and plenum volume would need a complicated mechanism as compared to varying valve timings and lifts. Mahindra 2 Wheelers [28] and Toyota's Acoustic Control Induction System (ACIS) [17, 29] are examples where different sets of runner lengths are used for lower and higher engine speeds. Variable runner diameter and variable plenum volume have not been so commonly used owing to the complexity of their manufacturing and integration. The most commonly implemented strategy is variable valve actuation (VVA). The common mechanisms that have been implemented in production are 2 or 3-step cam phasing for changing inlet valve timings and cam switching for changing intake valve lifts. Honda first introduced a 3-step cam mechanism to adjust valve lifts. Later they also introduced a cam phasing to their 2-step to adjust valve timings with respect to engine operation speeds [30]. BMW as well, with their 'Valvetronic' technology provides continuously variable valve lift and duration with cam phasing [31].

2: METHODOLOGY

To understand the application of the equations, an understanding of the pressure wave phenomenon should be acquired which is described in the following sections:

2.1: CHRYSLER'S RAM AIR THEORY

The motive of this theory is to capture the amplified pressure waves, as discussed above and create an induction boost. This is done by opening the intake manifold exactly when the high-pressure wave arrives near the intake valve as seen in Figures 2 and 4 [24, 25]. This can be done by changing the intake runner length or by changing the valve timing and duration. The lengths can be adjusted to get that extra pressure boost at the engine speed they are tuned for. Varying the intake runner lengths and valve timings can hurt the power of the engine as much as it can help. Hence proper variation of these parameters is very important [32].

When an engine is tuned, there is an increase in the pressure differential between the amplified pressure behind the intake valve and the negative pressure created on the other side of the valve due to engine's suction. When these high-pressure waves are released into the low-pressure combustion chamber, the mass flow rate of air into the cylinder is boosted thereby increasing the filling capacity of the engine and thus, the volumetric efficiency. This process is called as intake air ramming. It is also sometimes referred to as "acoustic supercharging" by race engineers [32].

Peak torque occurs at peak volumetric efficiency. Also, engine speed at peak torque corresponds to the that where a sudden surge in engine power is encountered [19]. So, the occurrence of peak torque and a sudden surge in engine power can also be controlled by varying the runner length, and valve timing [2, 8].

2.2: PRESSURE WAVE CAUSES

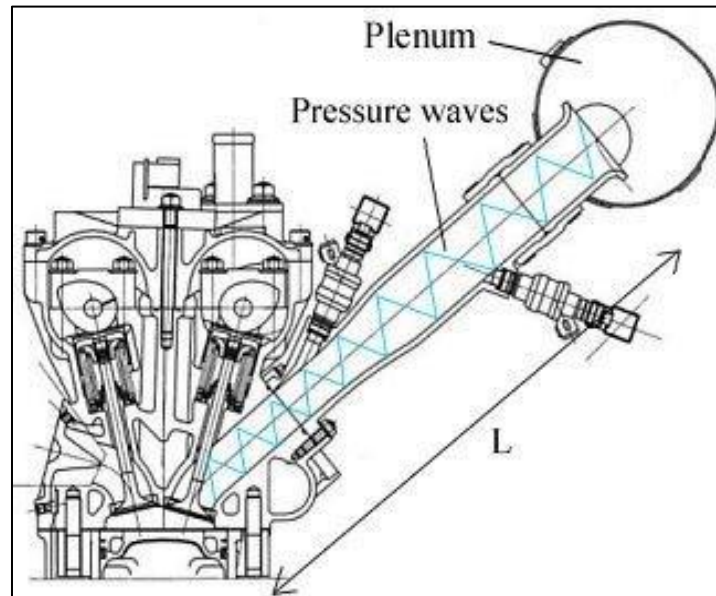


FIGURE 4: Pressure wave along intake runner [33]

There are three different phenomena causing a pressure wave in an engine as seen in Figure 4. The most commonly known cause of a pressure wave is the piston motion. On the intake stroke, the piston makes a negative pressure wave that travels from the piston to the plenum in the intake track. This negative pressure wave is reflected as a positive pressure wave from the plane where it finds an abrupt change in cross section i.e. the bell mouths or the plenum. This positive pressure wave travels back toward the cylinder. If it reaches the intake valve just before it closes, it will force a little more air in the cylinder. The second, less realized, cause of pressure waves is the exhaust. With a well-tuned exhaust system that scavenges efficiently, during the overlap period there will be a negative pressure wave as the exhaust is scavenging and pulling in fresh intake charge. This negative pressure wave would also do the same thing as the above-mentioned wave. If the intake runner length is correct for that engine speed, the reflected positive pressure wave will be

at the valve just prior to its closing event and increases air flow in the engine. The third and most compelling cause of pressure waves is valve closing event. The valve closing event creates a high-pressure sound wave. Also, any velocity left in the intake port column will create high pressure wave at the back of the valve. These high-pressure waves travel toward the open end of the intake tract and are reflected as a low-pressure wave. When this low-pressure wave reaches the intake valve and finds it closed, the wave reflects as non-inverted positive pressure wave itself. The idea of tuning is to adjust the length of intake runner and valve opening timing such that the positive pressure wave is just waiting to be released in the cylinder as soon as the valve opens [2, 8]. This would also increase the cylinder's filling capacity and increases the volumetric efficiency thus boosting engine performance [34].

2.3: PRESSURE WAVE SPEED

The pressure waves mentioned above have speed, tone and amplitude and they are amplified. The pressure waves travel at the speed of sound. In hot intake air (25 to 30 degrees Celsius) it will travel at about 1250 to 1300 ft. per second [2, 8]. The speed of these pressure waves is not a function of engine's operating speed and thus wave tuning only works in a narrow rpm range for a fixed intake assembly [34].

2.4: HELMHOLTZ RESONANCE THEORY

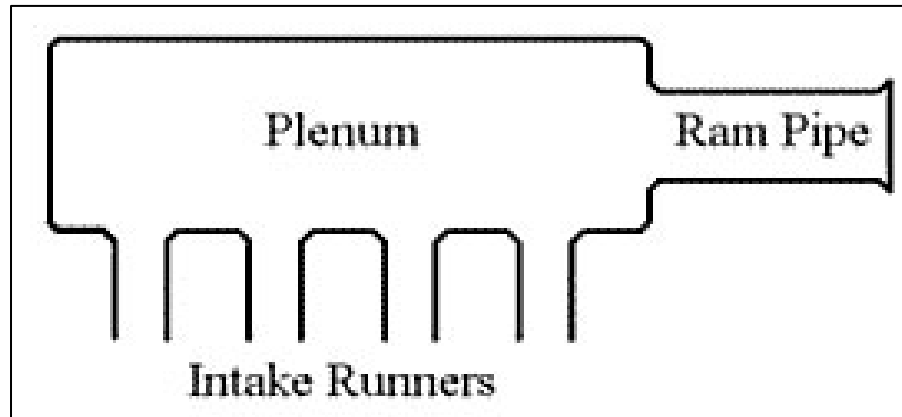


FIGURE 5: Plenum and Intake runner layout [24]

Helmholtz proposed a theory to continue to use the tuned port advantages in the plenum and intake pipe setup as seen in Figure 5. The tuned ports are Helmholtz resonators themselves. This theory provides an equation to tune the intake lengths also taking into consideration the need to reduce intake runner lengths by considering multiple reflections of the pressure waves [35]. When the intake valve is closed, port & runner system resonates like a closed-ended organ pipe, with a resonant frequency (Hz) of F_p expressed as Equation (2) [36]. The reflection at the open end of intake runner is out by half the intake pipe's diameter. Hence the effective runner length is more than the actual measured intake runner length by half times the average runner diameter.

$$F_p = \frac{c}{4 \cdot L_{\text{eff}}} = \frac{c}{4 \cdot (L + 0.5D)} \quad (2)$$

Where,

F_p = Resonant Frequency (Hz)

C = Speed of sound at intake temperature (ft/sec)

L_{eff} = effective length of runner (ft)

= (measured length (L) + 0.5* average runner diameter (D))

In the case when the intake valve is open, tuning-peak occurs when Helmholtz resonance of cylinder and runner as a combined system is almost twice the piston frequency. The port & runner system act as a single Helmholtz resonator as seen in Figure 6, with a resonant frequency (Fh) as expressed in Equation (3) [36].

$$F_h = \frac{c}{2\pi} \left(\frac{A}{L_{\text{eff}} * V} \right)^{\frac{1}{2}} = \frac{c}{2\pi} \left(\frac{A}{(V(L+0.5D))} \right)^{\frac{1}{2}} \quad (3)$$

Where:

A = Inlet pipe cross-sectional area (ft²)

L_{eff} = effective length of runner (ft), as above

V = effective cylinder volume (ft³)

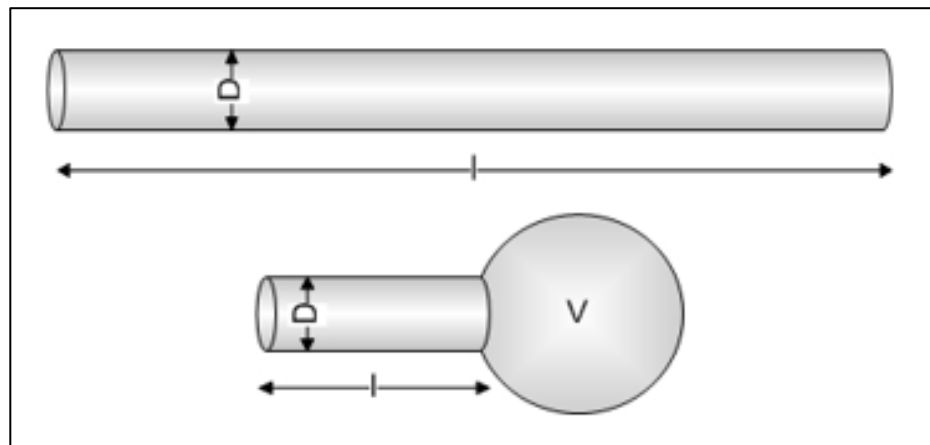


FIGURE 6: Plenum and intake runner diagram

For a four-stroke engine, the inlet valve is closed for 2 cycles (720 degrees of rotation) less the cam's inlet duration. However, the cam takes time to open and close. So, the effective cam duration (ECD) will be cam duration minus 20-30 percent. The length of the intake runners cannot be made long enough to capture the first reflection of the pressure wave due to the geometry constrains. Hence, the runner is designed to capture the pressure

wave after multiple reflections. The number of reflections after which the pressure wave is captured is called the reflection valve (RV). This can be expressed as Equation (4) [4, 12, 36].

$$L = \left(\frac{(720 - \text{ECD})C}{N * 2 * \text{RV}} \right) - 0.5 D \quad (4)$$

Where

C = Speed of sound at intake temperature (ft/sec)

ECD = Effective Cam Duration (Degrees)

N = Engine Speed (rpm)

RV = Reflection Value

D = average runner diameter (ft)

2.5: ENGELMANN'S FORMULA

The Helmholtz resonator method, and its derivatives, are being used substantially for over 60 years and major research in this field is still going on for the design of intake runners [13]. Using the Helmholtz theory and considering the engine cylinder dynamics, Engelmann was the first to propose the following Equation (5) which also proved to be more useful over a comparatively wider range of engine speeds [35, 37].

$$N = \left(\frac{162}{K}\right) * C * \sqrt{\frac{A}{LV}} * \sqrt{\frac{R-1}{R+1}} \quad (5)$$

Where,

N = Engine Speed (rpm)

K = 2.0 to 2.5 for most conventional engines

C = Speed of sound at intake temperature (ft/s)

V = Cylinder volume (in³)

L = Measured length of intake runner (in)

A = Inlet pipe cross-sectional area (in²)

R = Compression ratio

162 = Constant incorporating units

2.6 EFFECTS OF INTAKE VALVE OPEN AND CLOSING TIMINGS

As can be seen from Equation (4), the tuned intake runner lengths are a function of engine speed and valve open duration. So, this equation can be re-written as Equation (6) to get the same tuning effects by changing the valve timings and profile with respect to engine speed and maintaining the intake runner geometry constant [2, 8].

$$ECD = \left(\frac{(\text{rpm} \times RV \times L_{\text{eff}})}{(ECD \times 0.25 \times C \times 2)} \right) - 0.5 D \quad (6)$$

Where,

L_{eff} = effective length of runner (m)

= (measured length (L) + 0.5 × average runner diameter (D))

C = Speed of sound at intake temperature (m/s)

ECD = Effective cam duration (degrees of cam rotation)

N = Engine speed (rpm)

RV = Reflection Value

D = Average runner diameter (m)

The opening and closing of the intake or the exhaust valves with respect to the piston Top Dead Centre (TDC) and Bottom Dead Centre (BDC) is referred to as valve events. The intake valve is generally opened before the top dead center to facilitate exhaust gas recirculation (EGR). During the valve overlap period, when both intake and exhaust valves are open, the exhaust gases can flow into the intake manifold, rather than leaving the cylinder through the exhaust manifold. The resulting internal EGR would cause in-cylinder pressure to drop as cylinder descends after TDC and cause the exhaust gases to take place of the fresh air in the cylinder, thereby reducing the number of oxygen molecules available for the combustion of fuel. At part load conditions, this will reduce fuel

consumption and reduce NO_x emissions by limiting the peak cycle temperatures. However, increased EGR depending on the valve overlap period will also reduce the torque at full load conditions. Hence, controlling valve overlap period according engine speed is very important to maintain a balance of part load fuel efficiency and full load torque [9, 10, 26].

Intake valve lift and intake valve closing time decides the amount of air that can be trapped in the cylinder during the intake stroke. Ideally intake valve should close exactly when the maximum amount of air has been captured in the combustion chamber to get the maximum possible torque output. Pressure waves created during the intake stroke continue to keep filling the cylinder even after the piston has reached BDC. The reflection of these pressure waves back and forth in the intake tract gain them enough inertia to keep filling air opposing the upward motion of the piston. Advancing valve closing event before this point will prevent this extra air from entering the cylinder. Whereas retarding the valve event beyond this point will cause the inducted air to flow back into the intake manifold. In both the cases the volumetric efficiency of the engine will reduce hurting the performance and efficiency of the engine. Hence precise control over these pressure waves is very important. The coefficient of flow, kinetic energy and turbulence intensity of the air flowing through the intake valve govern the behavior of the induction wave created during suction stroke. Hence, varying valve lifts according to the engine speed will grant a precise control of the pressure wave and help to boost the volumetric efficiency, torque and thus fuel efficiency at all engine speeds [9, 10, 26].

2.7: ENGINE SELECTION

In older carbureted engines, fuel is mixed with air in the intake runner at a much earlier stage prior to entering the cylinder. Since, vaporized fuel is denser than air, the air and vaporized fuel flow with different velocities leaving behind the vaporized fuel at sharp edges and bends, making the mixture heterogeneous and disturbing the flow in the intake runners [18]. A port injected, or gasoline direct injected engine will also allow us to isolate and observe the ramming and the pressure wave tuning effects in the intake runner. A high revving engine will allow us to investigate the effects of variable length runners and variable valve timings separately at low, medium and high engine speeds. An electronically controlled injection and ignition system, would nullify the other uncertainties and disturbances like drop in engine speeds with increase in load.

The 510 cc KTM Duke EXC single cylinder internal combustion engine selected for this study is a short stroke high performance high revving electronically port injected qualified for all the necessary requirement. Moreover, the single-cylinder configuration of this engine will make it easy and cost-effective to build an experimental set-up to validate the results of this thesis. The engine top speed and the power developed per unit weight (power to weight ratio) are high enough to call it a pre-tuned performance engine. Hence, any further improvement seen in the engine performance can be assumed to be solely because of the changes introduced in the air-induction assembly. The engine also uses a readily available moderately priced fuel i.e. Gasoline. This would make the engine testing economical. The engine specifications are shown in Table 1.

TABLE 1: Engine Specifications [38].

Number of Cylinders		1	
Bore		95mm	
Stroke		72mm	
Length of Connecting Rod		122.4mm	
Compression Ratio		11.9:1	
Number of Valves		4	
Intake	Number of Valves		2
	Valve Diameter		40 mm
	Valve Lift		9.62 mm
	Stock Port Length		460 mm
	Length of Variable Section		350 mm
Exhaust	Number of Valves		2
	Valve Diameter		33 mm
	Valve Lift		8.58 mm
	Stock Port Length		573 mm
Fuel Delivery		Port Injected	
Fuel Type		Indolene	
Air/Fuel Ratio		14	
Valve Timings	Intake	Open	13° Before top dead center
		Close	72° After bottom dead center
	Exhaust	Open	109° After top dead center
		Close	36° After top dead center
Heat Transfer Model		Woschni Heat Transfer	
Combustion Model		SI Wiebe Combustion	

2.8: 1-D SIMULATION MODEL

Engine simulation software is developed to reduce the cost of development by shortening testing time and effort required to reach the desired results. The simulation software used in this research is the market leading ISO approved, 1-Dimensional (1-D) engine and gas dynamics simulation software Wave from Ricardo. Ricardo Wave enables performance simulations to be carried out for steady-state as well as transient simulations applicable to virtually any intake, combustion and exhaust system configurations. To investigate the concept of representing the KTM internal combustion engine in 1D in Wave, all the parameters of the engine are measured and modelled. Some of the parameters are obtained from the engine manual [38]. The procedure is to split the three dimensions into multiple one-dimensional data. This is done with the pre-programmed equations in the software. For the software to be able to solve given tasks, coefficients and advanced sub-models are implemented. With user-provided data, pre-programmed equations and governing laws of physics like momentum, energy and mass transfer, different performance parameters of a particular engine under variable operating conditions can be simulated and results like fluid pressures, temperatures, volumetric efficiency, power, torque curves, pressure-volume diagram, heat-release diagram etc. can be obtained. [39, 40]

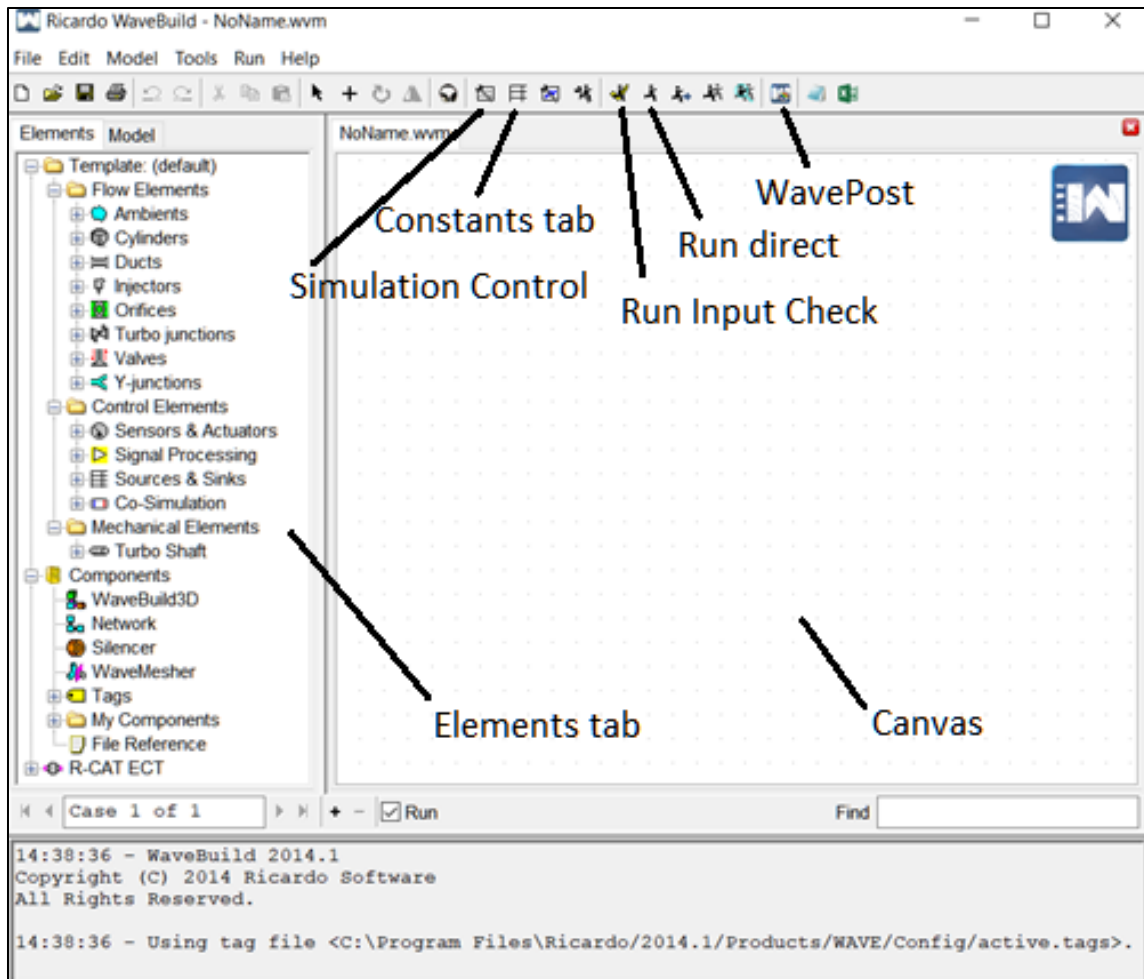


FIGURE 7: Ricardo Wave Build Window at startup

Ricardo Wave Build interface seen in Figure 7 consists of a blank canvas where the required components can be dragged and dropped from the pallet window (element's tab) on the left side of the canvas. The properties of each component can be edited by double clicking on the component in the canvas. The default unit system uses is SI unit system. However, the unit for each input are displayed besides the entry fields from where it can be changed if desired.

The flow field is not reinitialized in between each case by default because final conditions for a converged case are generally closer to initial cases than the subsequent cases (temperature, pressure, velocity and others). But, since a batch simulation is going to

be run in this case, flow field must be reinitialized for each case which can be done in the simulations control tab. The simulations controls tab (Figure 8) also provides the options to control the dynamics of the simulation like the tolerance to be considered while detecting convergence of results. Reducing the tolerance will make the simulations faster but will reduce the accuracy of results. Hence, stating proper simulation controls is very important to get reliable results from the software. A standard tolerance of 0.01 units for convergence has been set here. The initial wall-friction and heat transfer multipliers are initially set to 1. They are used to refine the model to match the experimental results, once the entire model is built.

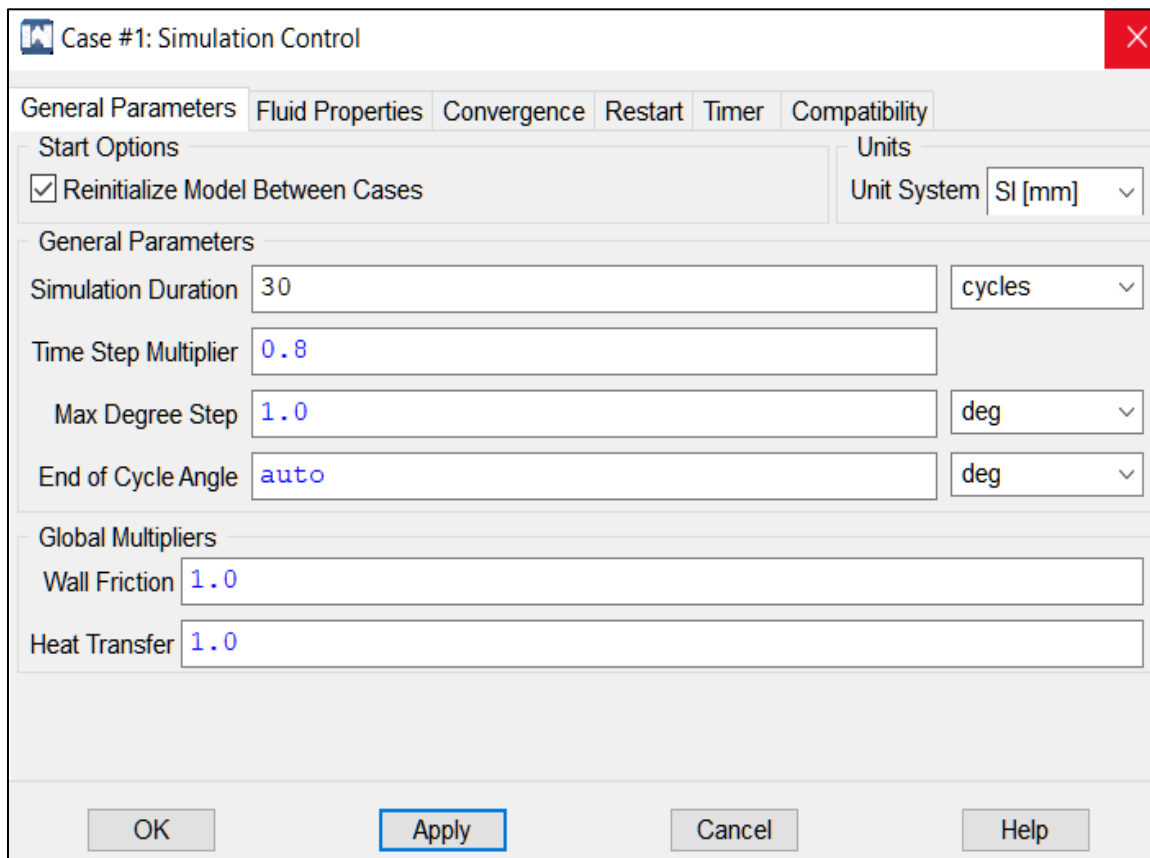


FIGURE 8: Simulation Control Tab

The fuel properties can also be set from the simulations control tab. Fuel properties define how the fuel and air react as a function of temperature, pressure and concentration. Based on these properties, Wave tracks five species, fresh air, burned air, vaporized fuel, burnt fuel and liquid fuel respectively. The engine being modelled works on gasoline. Indolene display remarkably similar combustion and evaporation characteristics as commercial 87 octane rated (no ethanol) unleaded gasoline [41] . Hence, Indolene which is the closest match to gasoline from the available templates for fuel properties, is selected as a fuel for all the simulations.

Once done with specifying the simulations control, modelling can be started by dragging and dropping components like the cylinder, junctions, orifices, ambient air, injectors, butterfly valves and others to the canvas. These components are to be joint by ducts. The properties of each components can be specified by double clicking on the components. Once the model is completely built it should look like Figure 9.

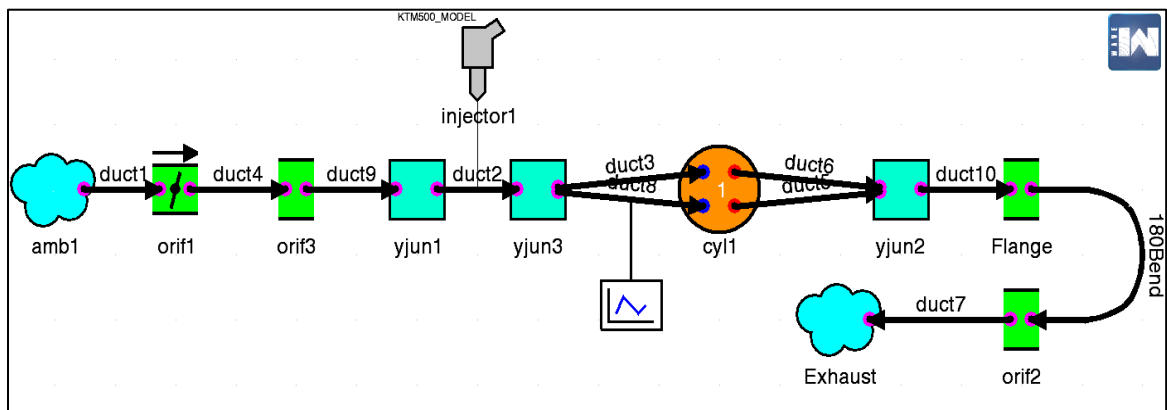


FIGURE 9: 2-D model of the engine

The initial ambient are set. The ambient temperature and pressure are set to 300 K and 1 bar. 100% fresh air supply is assumed as an initial condition. The discharge co-

efficient for all ducts, orifices and junctions is set to AUTO and is calculated automatically by Wave using Equation (7)[42].

$$CD = 1 - \left[1 - \left[\frac{D}{D_1} \right]^4 \right] * \left[0.2 + 0.2 \left[1 - \left[\frac{D}{D_2} \right]^4 \right] \right] \quad (7)$$

where,

CD = Discharge co-efficient

D = Orifice diameter

D₁ = Upstream diameter

D₂ = Downstream diameter

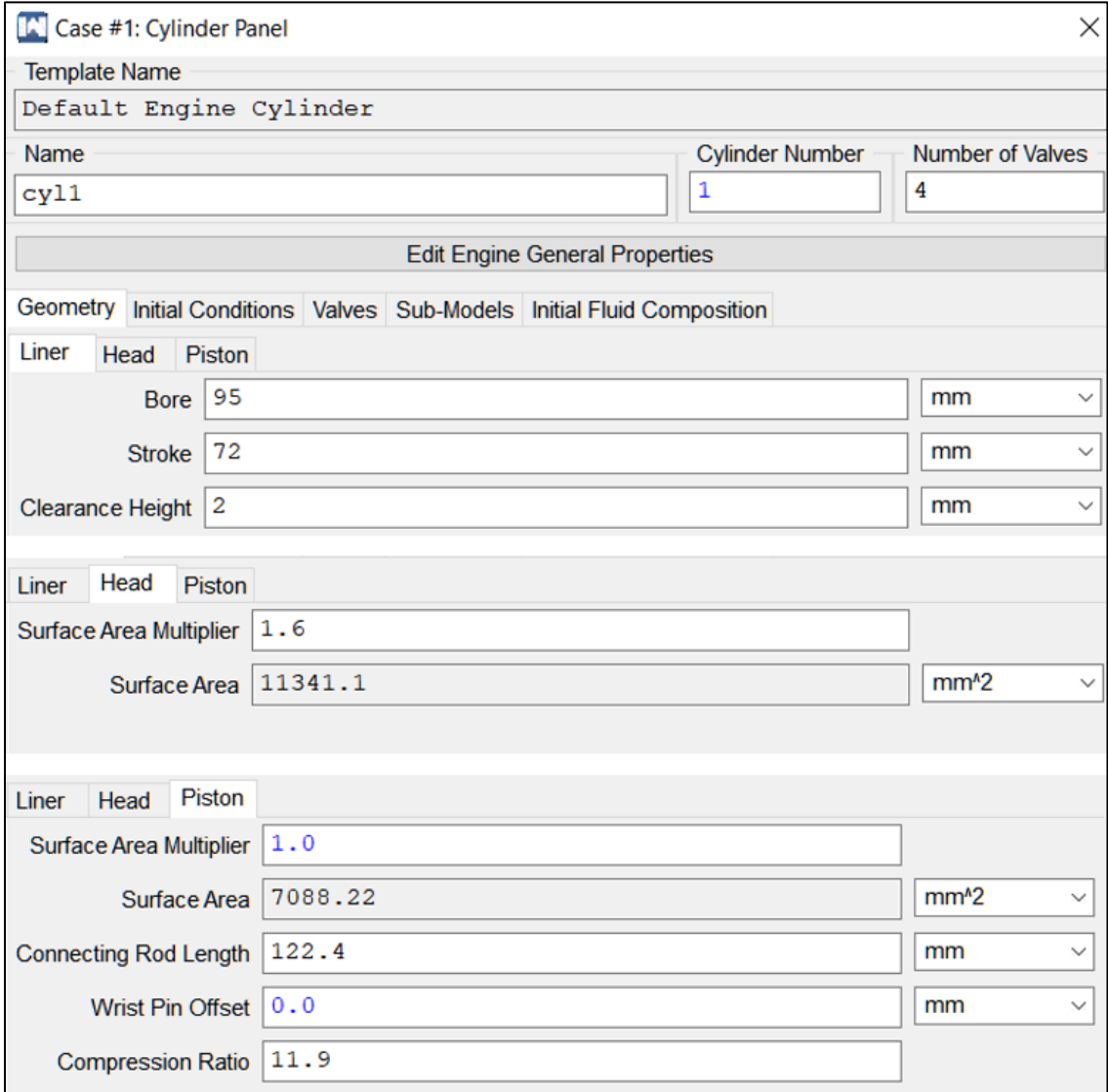
The intake system comprises of a butterfly type throttle valve which is set at wide open position (WOT) i.e. 90° throughout all the simulations. It also consists of a convergent divergent nozzle whose upstream diameter is 42 mm, had a 20 mm restrictor at its throat and has a downstream diameter of 43 mm. This restrictor is added as this engine is used for Formula Student Race Car (FSAE) events and has an intake track designed in such a way to comply with the rules of the FSAE competition. This divergent part of this nozzle opens to a plenum/ air-box of 3-liter volume. Downstream of the air box is the intake runner. The intake runner is assumed to have a uniform diameter of 42.86 mm. The assumption that the runner diameter is constant is made to avoid complexities in modelling and further tuning the engine. The error in modelled performance that may arise due to this assumption can be eliminated by changing the heat transfer and friction co-efficient multipliers during the validation part, after the entire model is ready. As it can be seen in Figure (9), the intake runner is divided in three parts. First part is the part of the runner which can be varied. Downstream of which is the second part is where fuel is injected. Further downstream is the third part where the intake runners are divided into two different

runners going to each intake valve. The second part and the third part have fixed geometry throughout all the simulations. Their combined length and diameter are maintained at 250 mm and 42.86 mm respectively. They are joint by a Y-Junction. The length of first part which is downstream to the air-box can be varied from 0 to 200 mm. This is the part of the intake runner which will be subjected to variations during further simulations. The intake runner is modeled in such a way for the ease of simulating engine performance with variable runner lengths. Also, since the injector location with respect to the intake valve is now fixed, all the performance variations which could have aroused due to injector location variations have been eliminated. The injector location specified to be 5 mm downstream the starting point of the second part of the runner and the initial air-fuel ratio is set as 14:1.

Sensors can be added in the model to measure the pressure and temperature at various points. A pressure sensor is mounted to monitor the local pressure at the point where the air enters the combustion chamber. This sensor should have ideally been mounted directly on the end of the intake runner just before the intake valve. However, the sensor is mounted 5 mm before the runner meets the valve owing to the limitations of the simulation software. Another pressure and temperate sensor is mounted inside the combustion chamber to monitor the in-cylinder pressures and temperatures at all speeds and load conditions.

The exhaust system on the other hand is very simple. It starts with two runners downstream of the engine, being unified in a single duct by a Y-junction, followed by a duct with a 180° bent. Downstream of this is an expansion chamber which is designed to do the work instead of a muffler which leaves the air to the atmosphere. The ambient air outside the exhaust is given the same initial conditions as the ambient air at intake.

To define the characteristics of the engine cylinder, all the engine dimensions including the bore, stroke, number of intake and exhaust valves, clearance height, and length of connecting rod are entered in the appropriate fields in the cylinder panel seen in Figure 10.



Case #1: Cylinder Panel	
Template Name	Default Engine Cylinder
Name	cyl1
Cylinder Number	1
Number of Valves	4
Edit Engine General Properties	
Geometry Initial Conditions Valves Sub-Models Initial Fluid Composition	
Liner Head Piston	
Bore	95 mm
Stroke	72 mm
Clearance Height	2 mm
Liner Head Piston	
Surface Area Multiplier	1.6
Surface Area	11341.1 mm ²
Liner Head Piston	
Surface Area Multiplier	1.0
Surface Area	7088.22 mm ²
Connecting Rod Length	122.4 mm
Wrist Pin Offset	0.0 mm
Compression Ratio	11.9

FIGURE 10: Cylinder Panel

The friction mean effective power (FMPE) is calculated by Wave using the Chen-Flynn friction correlation model. Equation (8) is used to calculate FMPE and the recommended

values for the Chen-Flynn correlation coefficients are to be entered in the Engine general properties panel as shown in Figure 11.

$$\text{FMEP} = \text{ACF} + \text{BCF}(\text{Pmax}) + \text{CCF} \left(\text{RPM} * \frac{\text{stroke}}{2} \right) + \text{QCF} \left(\text{RPM} * \frac{\text{stroke}}{2} \right)^2 \quad (8)$$

where,

ACF= constant portion of the Chen-Flynn friction correlation

Pmax= peak cylinder pressure

BCF= account changes in Pmax, varies linearly with peak cylinder pressure

CCF= term which varies linearly with the piston speed, accounts for hydrodynamic friction in the power cylinder

QCF= term which varies quadratically with the piston speed, accounts for windage losses in the power cylinder

stroke= cylinder stroke

Friction Correlation	
ACF	0.35 bar ▾
BCF	0.005
CCF	400 Pa*min/m ▾
QCF	0.2 Pa*min^2/m^2 ▾

Figure 11: Chen-Flynn friction correlation coefficients

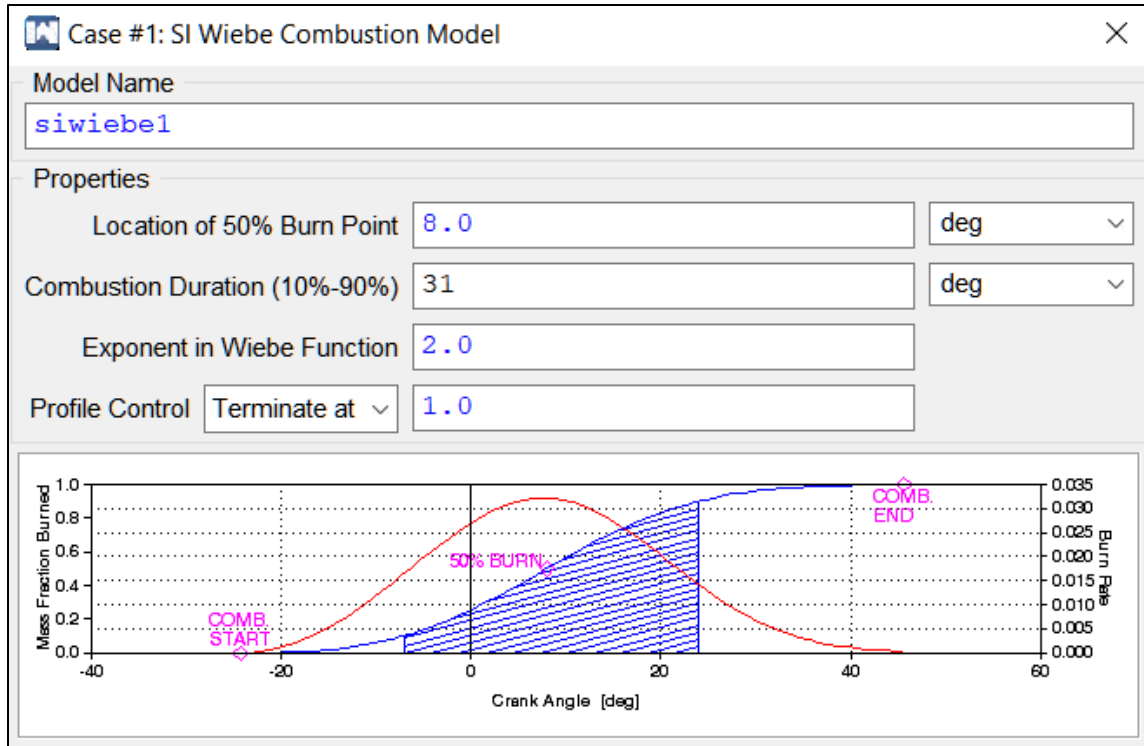


FIGURE 12: SI Wiebe combustion submodel

The combustion and heat transfer model are also selected from the engine general properties panel. Wave provides the options to use one of the four combustion sub-models viz. Profile, SI Wiebe, Multi-Component Wiebe, and SI Turbulent Flame sub-models. Profile sub-model can be used if the fuel mass burn rate with respect to engine crank angle is known for every speed and load point. Multi-Component Wiebe is used for the non-conventional combustion systems by overlaying multiple burn patterns to form a complex burn profile. SI turbulent sub-model is a predictive combustion sub-model used in complex advanced simulations. The most widely used sub-model is the SI-Wiebe, in which a S-curve function representing the fuel mass burn rate with respect to time is used [42]. The SI-Wiebe is selected as the combustion sub-model as this would be the best-fit for this research. The SI Wiebe combustion sub model window is shown in Figure 12.

Woshini Correlation heat transfer model is used in these simulations. This is the most commonly used sub model. It assumes that the heat transfer of a confined volume through all the surrounding walls. In this case it will assume the heat transfer through the piston face, cylinder walls, head, valves, etc. The area available for heat transfer for these components is calculated using the dimensions and ratios given when the parts were defined.

Intake and exhaust valves are modelled as global valves. This means that all the intake valves will have the same geometry, timings and motion profiles and the exhaust valves will have the same geometry, timings and profile. The lift profile of the engine valves is measured using a dial gauge against engine crank angle. The intake and exhaust valve profiles for setting up the stock simulations are as seen in Figure 13 and Figure 14, respectively.

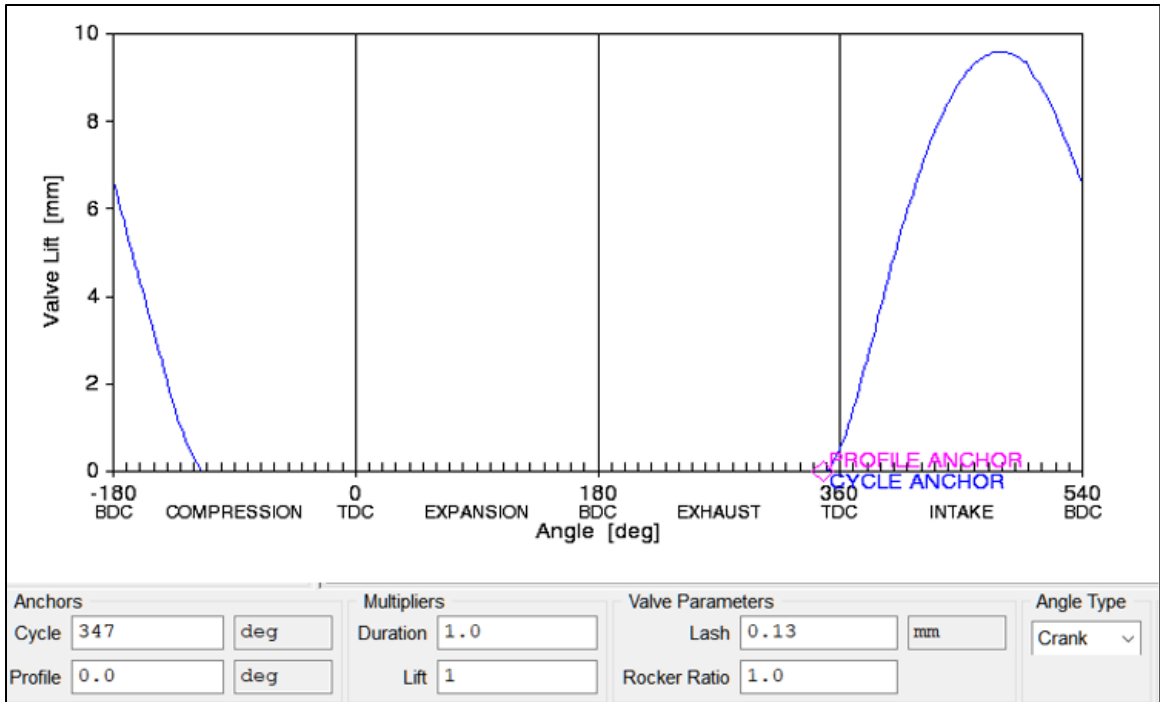


FIGURE 13: Intake valve profile

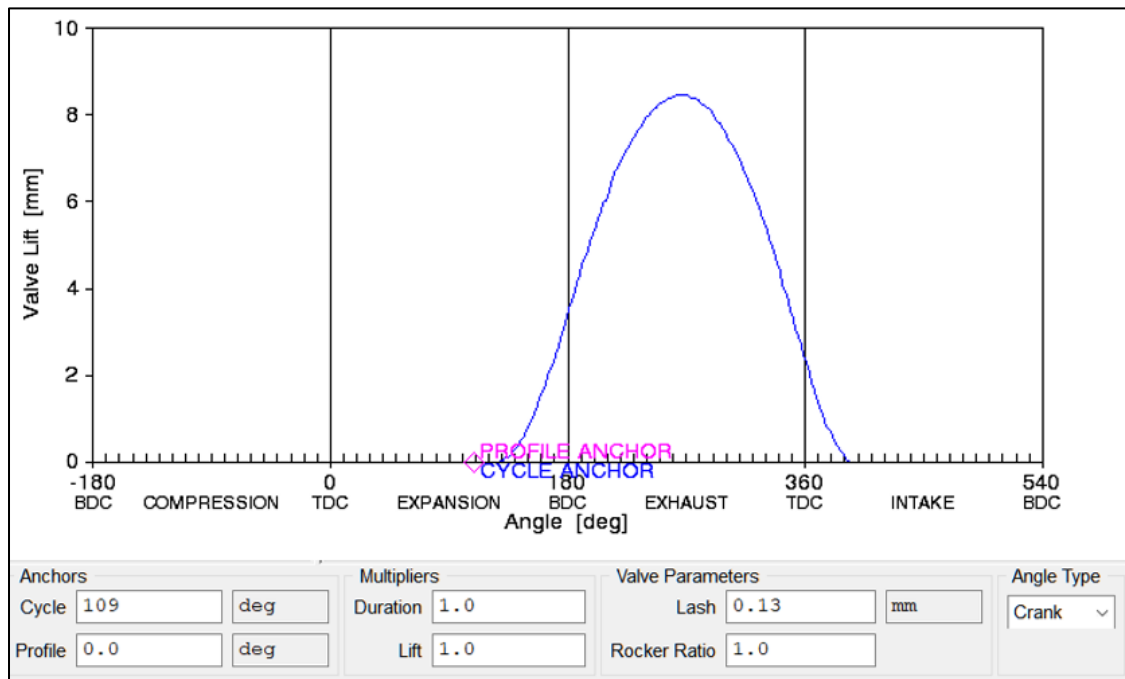


FIGURE 14: Exhaust valve profile

2.9: VALIDATION OF THE MODEL

Figure 9 shows the 2-D model of the engine, modelled as per its factory (stock) dimension. The model is altered at a few places to match the experimental data obtained by testing the engine on a chassis dynamometer from 5500 rpm to 7500 rpm with an average accuracy of 98%. The simulated engine power and engine torque are plotted against experimental results as can be seen in Figure 15 and Figure 16.

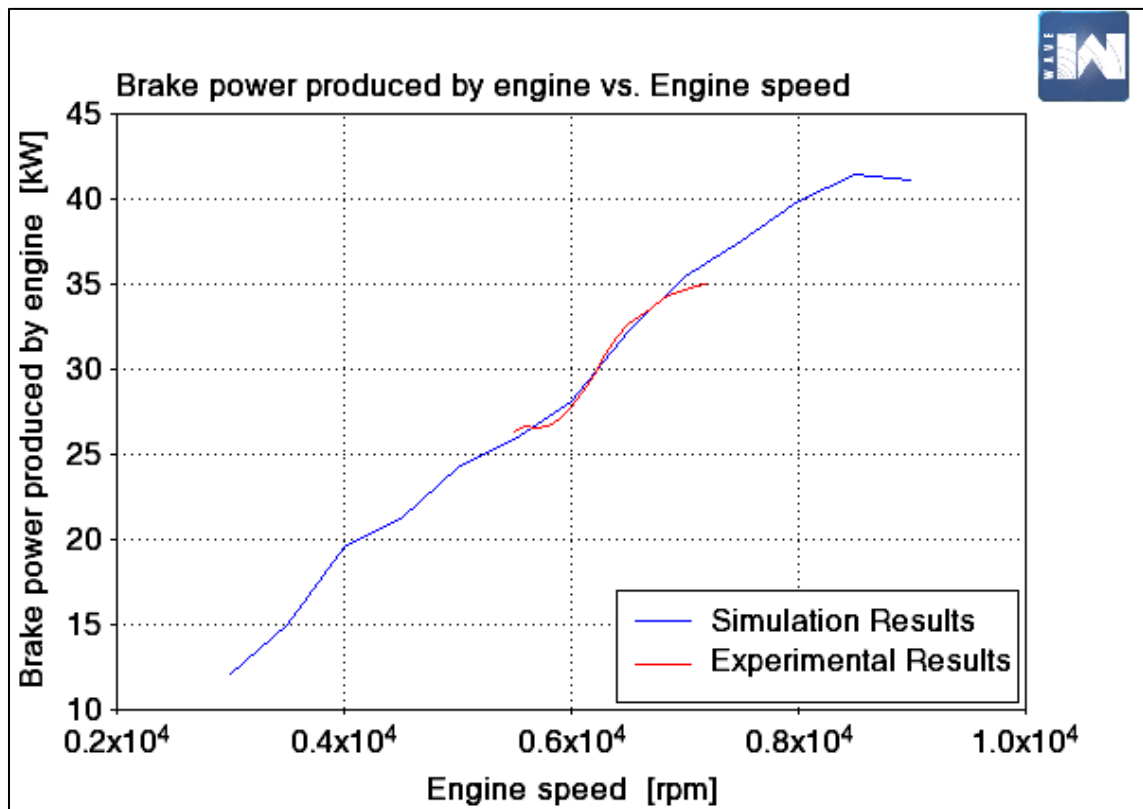


FIGURE 15: Brake power v/s engine speed - Simulation results validated against experimental power

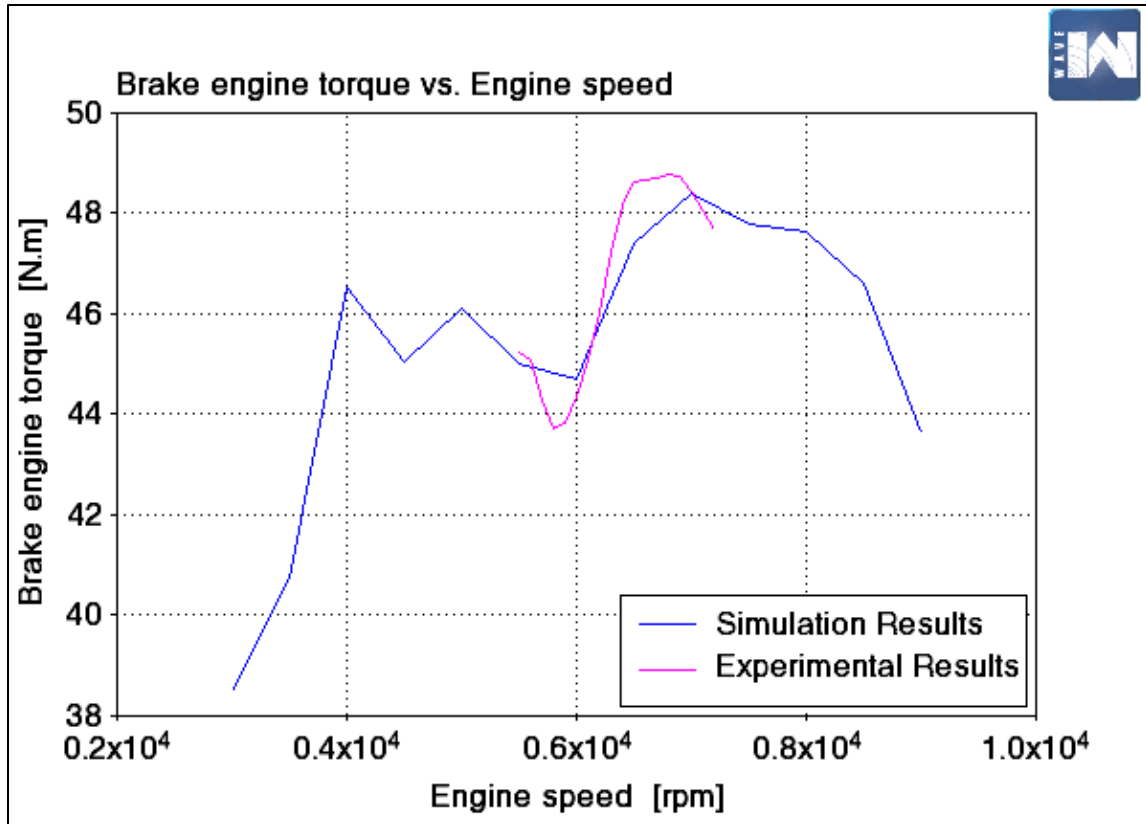


FIGURE 16: Brake torque v/s engine speed - Simulation results validated against experimental power

Engine power and torque, the most important performance parameters of an engine are usually measured using an engine dynamometer. According to Sodr  Et. Al, the expected standard uncertainty could be around 0.1kW for power and 0.15 Nm for torque in experimental results [43].

The values achieved by a simulation are however believed to be unrealistic most of the times as they do not account for uncertainties that could be faced with practical testing conditions. Because of which simulations always tend to over-promise and corresponding experimental tests tend to under-perform.

To cope up with this issue of uncertainty, it is important to introduce the factor of uncertainty in the simulations. One of the ways to do this is to account for the uncertainties

in the values that are fed as input to the simulation software and then propagate these uncertainties to deduce the combined standard uncertainties in the output parameters given by the simulation.

The uncertainties associated with the measurement of input parameters like ambient temperature, ambient pressure, wall temperatures, intake and exhaust diameters, plenum volume, air-fuel ratio, injector location, angle of throttle valve, heat transfer co-efficient, friction co-efficient, and others are determined by Type-B evaluation. A Type-B uncertainty evaluation is the one which determines uncertainty of the basis of scientific judgement and is not done by using statistical methods of uncertainty evaluation [11].

These input parameters along with the pre-defined models used to model friction losses, combustion, heat transfer and turbulence models can be varied within their expected range of uncertainties and multiple simulations should be carried out. The data set if all the above parameters are varied will be very huge and beyond the scope of the study for this project. Hence, the uncertainties that could have been present in the geometrical dimensions of the engine components are neglected. Also, the in-cylinder and duct temperatures and pressures are defined as a function of ambient temperature and pressure, they need not be varied individually. Hence the only major contributing factors to the engine's performance that were varied were ambient temperature, pressure, wall friction co-efficient and the heat- transfer co-efficient. These are also the major input quantities for the turbulence, momentum, and heat transfer and combustion models used to simulate the engine performance by the engine simulation software. The parameters which are varied, and their respective uncertainties used for this analysis are shown in Table 2.

TABLE 2: Dominant input parameters used for uncertainty evaluation

Parameter	Value	Uncertainties (Type-B)
Ambient Intake & Exhaust Temperatures	300 K / 900K	2K / 4K
Ambient Intake & Exhaust Pressures	1 bar / 1.05 bar	0.01bar / 0.03bar
Heat Transfer Co-efficient	1	0.5
Wall Friction Co-efficient	1	0.5
Throttle Angle (degrees)	90 degrees	0.05 degrees
Air Fuel Ratio	14.7	0.5

Followed by this, a Monte-Carlo (Type-A) simulation is carried out where the input parameters are varied randomly within their uncertainty range and the 81 data points for engine power are obtained. The data points are found to be distributed as shown in the normal probability plot shown in Figure 17 and Figure 18.

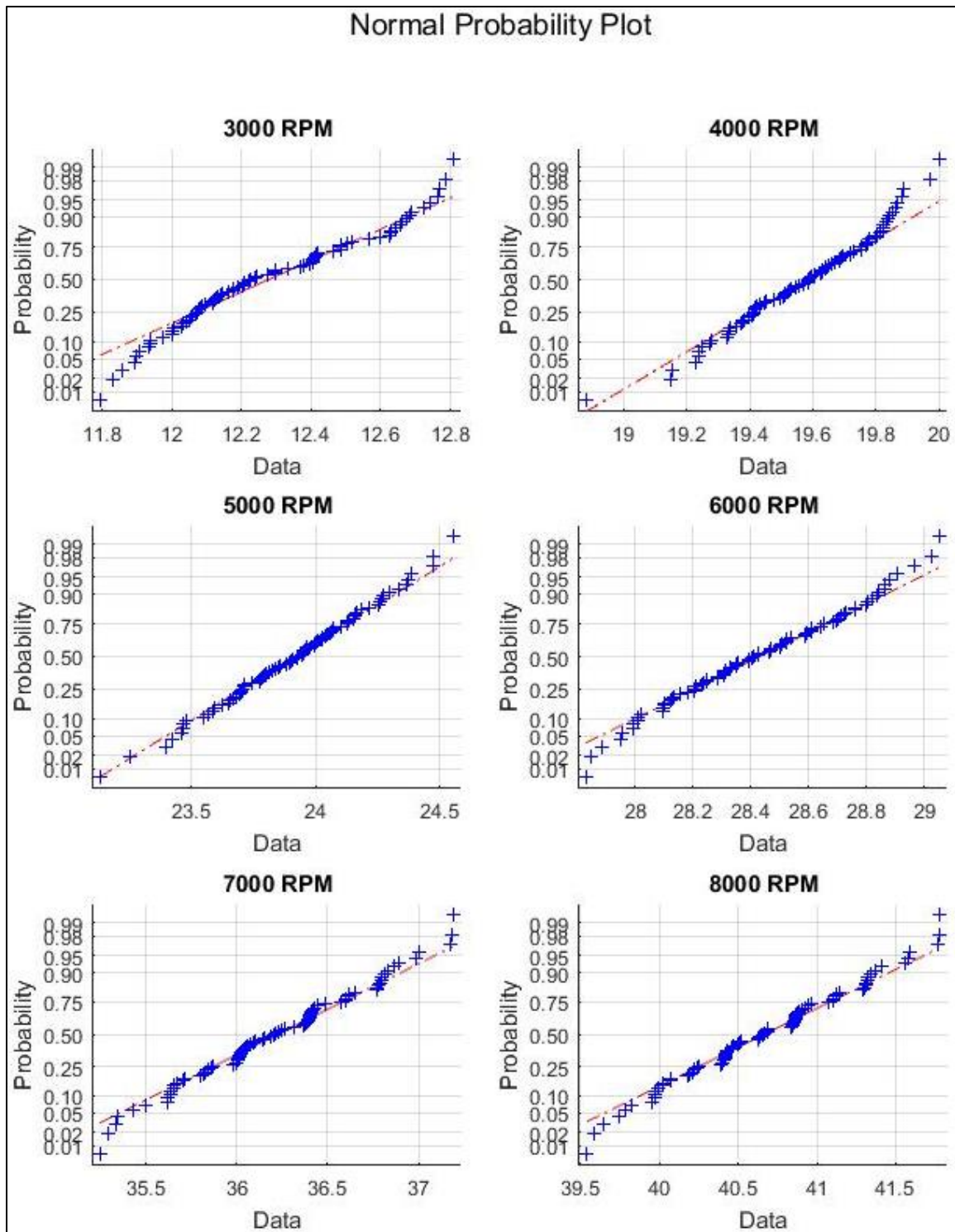


FIGURE 17: Normal probability distribution plots at each engine speed simulated (rpm)

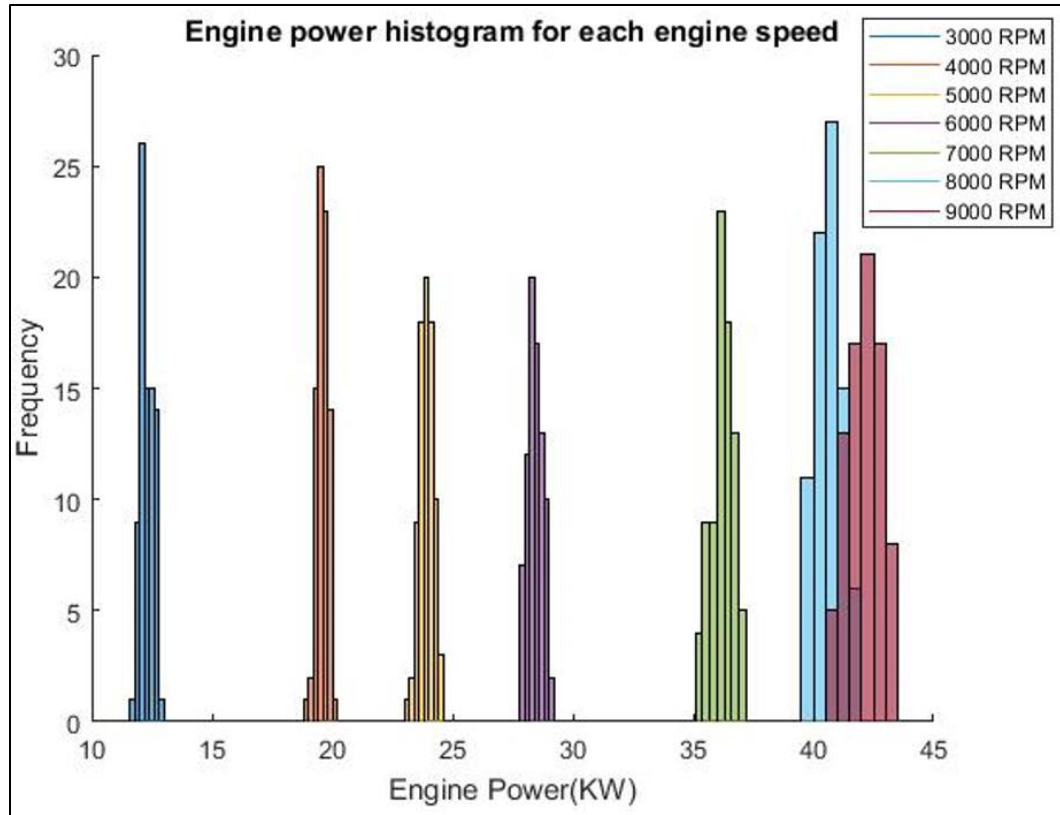


FIGURE 18: Engine power histogram for each engine speed

As it can be seen from the above two plots, the results are found to be distributed almost normally for each engine speed. This suggests that the Monte-Carlo simulation is successful, and values of uncertainty thus obtained are acceptable. Table 3 shows the results for the uncertainty analysis.

TABLE 3: Combine standard uncertainty of simulated power at each engine speed

Engine Speed (rpm)	3000	4000	5000	6000	7000	8000	9000
Combined Standard Uncertainty	± 0.27	± 0.22	± 0.29	± 0.30	± 0.47	± 0.55	± 0.67

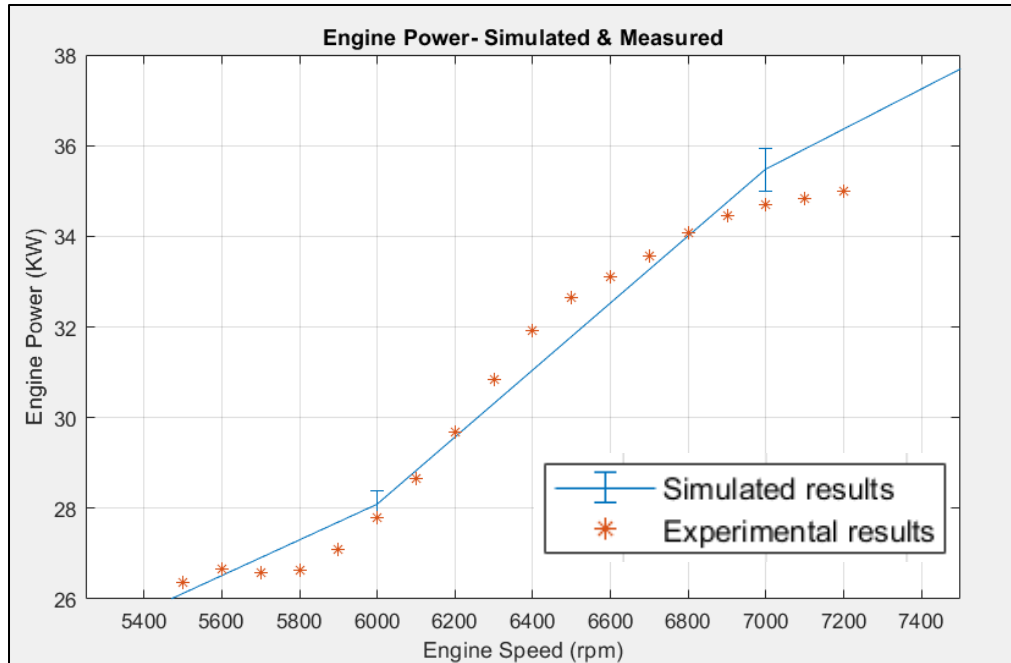


FIGURE 19: Comparison of simulated and experimentally measured engine power

(Coverage factor = 1)

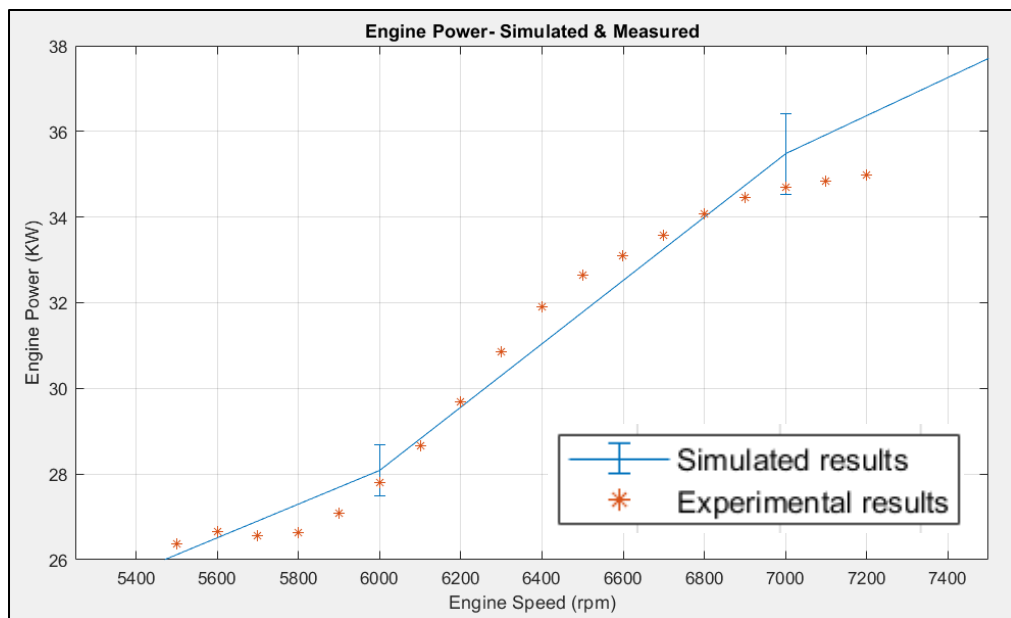


FIGURE 20: Comparison of simulated and experimentally measured engine power

(Coverage factor = 2).

To observe if the new estimated values of engine power are better than the earlier estimated values, engine power is re-plotted against engine speed with its uncertainty bars in Figure 19 with a coverage factor of 1. The coverage factor of 1 suggests that these are 64% confident results since the obtained data set is normally distributed.

From Figure 19 we can see the comparison of the simulated engine power and the experimentally measured engine power. When the error bars showing the combined standard uncertainty up to 1 standard deviation are plotted, most of the experimental points are also covered, but not all.

Hence another plot of engine power vs speed with expanded uncertainty of two times standard deviations is plotted. These results with a coverage factor of 2 are 98% confident results for since the obtained set of data points are normally distributed. Now it can be observed from Figure 20 that all the experimental points are covered by the error bars. This suggests that the uncertainty analysis was successful, since all the simulated data points lie within the uncertainty limits.

2.10: CASE SET-UP FOR FURTHER SIMULATIONS

The optimization process for achieving peak performance is carried out in 4 steps:

- Varying runner length dimensions to optimize volumetric efficiency
- Varying intake valve timing to optimize volumetric efficiency
- Varying intake valve lift to optimize volumetric efficiency
- Varying air-fuel ratio to match engine's original performance to optimize thermal efficiency

The parameters that need to be varied can be given different variable names and the can be varied in the constants tab. The engine performance is simulated and monitored after every 500 rpm for the variations in intake runner length, valve timings and valve lifts as shown in Figures 21-23.



FIGURE 21: Simulated runner lengths

The runner lengths are varied from 250 mm to 450 mm with steps of 5 mm. The runner lengths at which maximum volumetric efficiency is encountered are recorded for each engine speed. It would be difficult to use different runner lengths at every speed due to manufacturing and space constraints. Hence, brute force is used to divide the rpm range in two sets and select an optimum runner length for each set of engine speeds.

After selecting the optimum runner lengths to maximize volumetric efficiency, the intake valve opening time is varied from 290 degrees to 374 degrees after bottom dead center (BDC) with steps of 3 degrees to vary the valve overlap time. This wide range of valve opening time would help to analyze the effects of valve events and varying overlap throughout the engine operating speed range. Figure 22 shows the minimum and maximum overlap period simulated. The valve timings that give optimal volumetric efficiency are also found to differ at all engine speeds just like runner lengths. Hence the same algorithm is also used to divide the engine speed in two ranges and find the best fit valve times for each set.

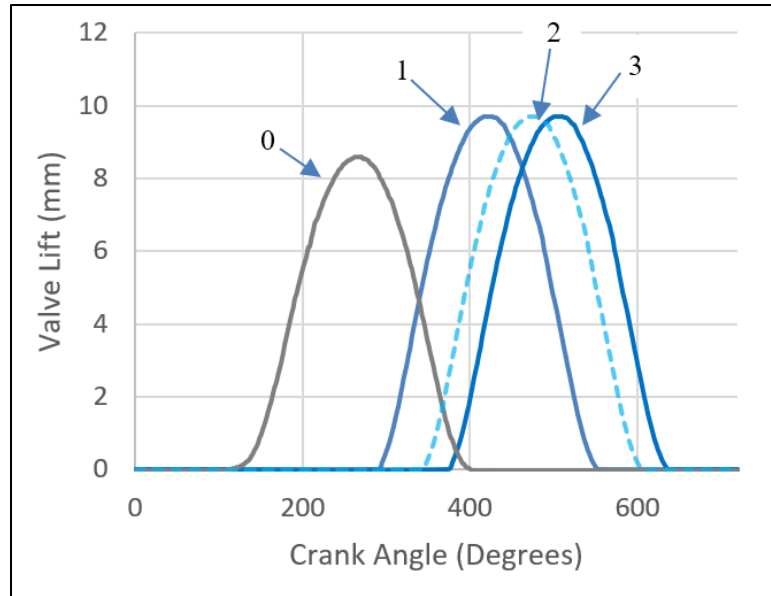


FIGURE 22. Simulated valve opening time range

Where

0 – Exhaust valve profile

1 – Most advanced valve opening timing

2 – Baseline valve opening event

3 – Most retarded valve opening timing

After optimizing the intake valve timings, the valve lift is varied by varying the valve lift multiplier from 0.8 to 1.2 with steps of 0.02. Figure 23 shows the range of valve timings where the engine performance is simulated for each engine speed. Just like the intake runner lengths and valve timings, the same algorithm is also used to divide the engine operating speeds in two sets and select the best valve lifts for each set.

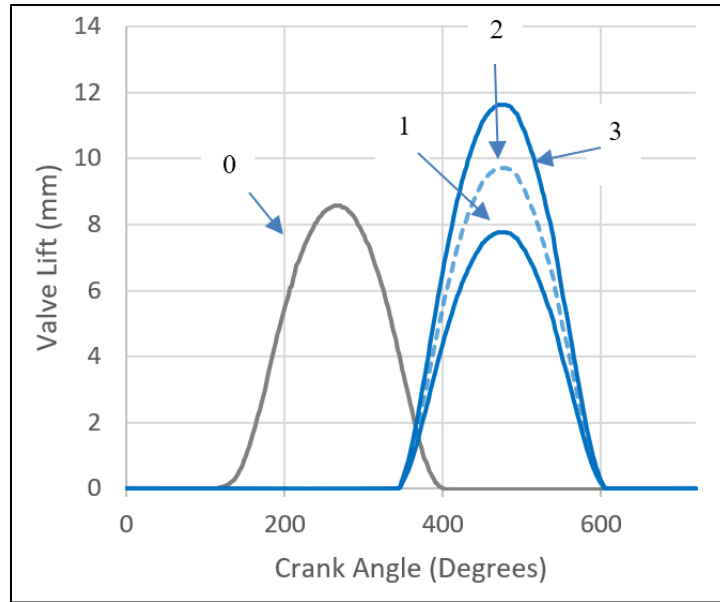


FIGURE 23. Simulated valve lift range

Where

0 – Exhaust valve profile

1 – Least valve lift

2 – Baseline valve lift

3 – Highest valve lift

Once, the runner lengths, valve timings and valve lifts delivering optimized engine performance are found, the air-fuel ratio is varied from 12 to 17 with steps of 0.05. The set of air-fuel ratios that would make the engine perform. The engine is run on variable air fuel ratios for all engine speeds and the set of air-fuel ratios which make the engine perform as it originally does are found. The engine with the optimized intake assembly power now performing almost like the engine with stock/ factory fitted intake assembly, the effects of tuned manifold on the thermal efficiency of the engine are observed.

3: RESULTS AND DISCUSSION

3.1: EFFECTS OF VARYING RUNNER LENGTHS

As mentioned earlier the engine performance is simulated from 3000 rpm to 9000 rpm and is recorded after the span of every 500 rpm.

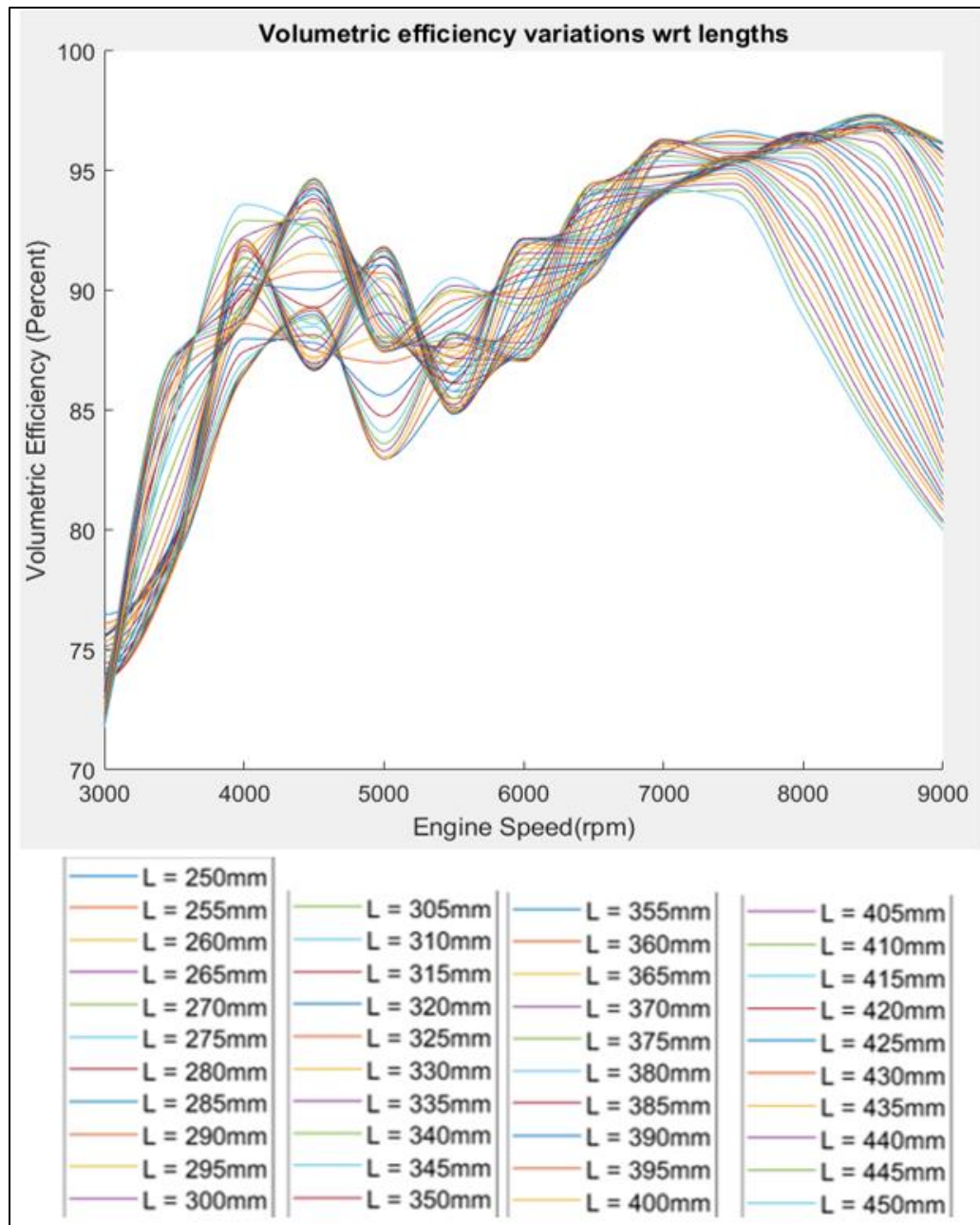


FIGURE 24: Variations is volumetric efficiency with respect to intake runner lengths

The runner lengths are varied from 250 mm to 450 mm in steps of 5 mm and the resulting variations in volumetric efficiency are shown in Figure 24. As can be seen from Figure 24, the volumetric efficiency of the engine is highly sensitive to changes in intake runner lengths. Since the volumetric efficiency of the engine has been simulated at all engine speeds for multiple runner lengths the plots are so intertwined. The most ideal plot for volumetric efficiency would be the one that would be plotted joining the peak volumetric efficiency that occurs at each engine speed. To get the optimized performance from the engine, variations in runner lengths would be required for each engine speed.

The set of optimal runner lengths to achieve peak volumetric efficiency at each engine speed and the resulting volumetric efficiency is shown in Figure 25 and Figure 26 respectively.

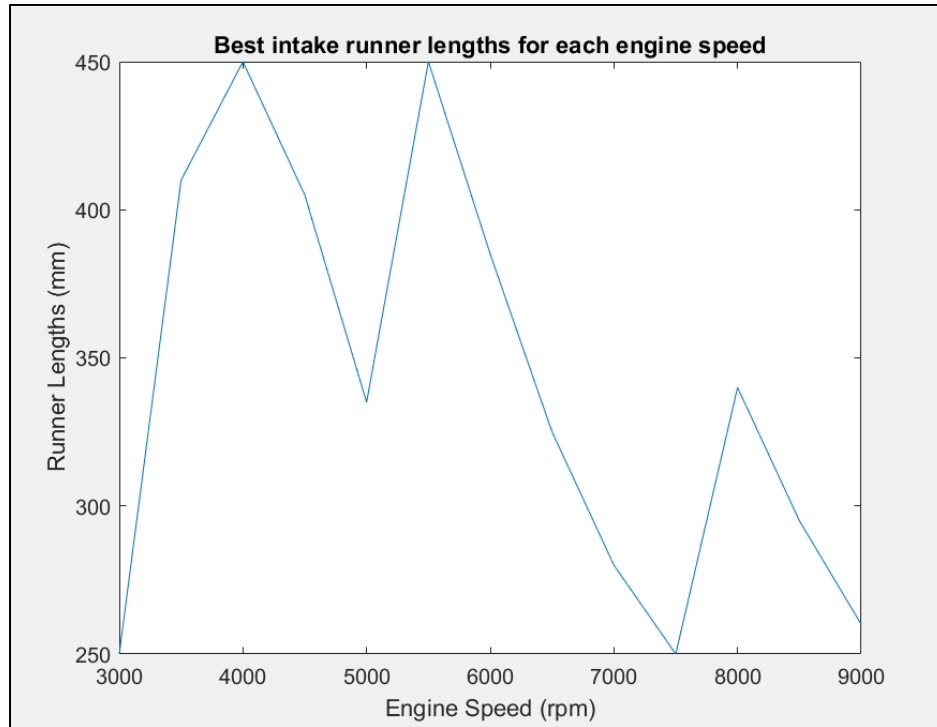


FIGURE 25: Best intake runner lengths for each engine speed

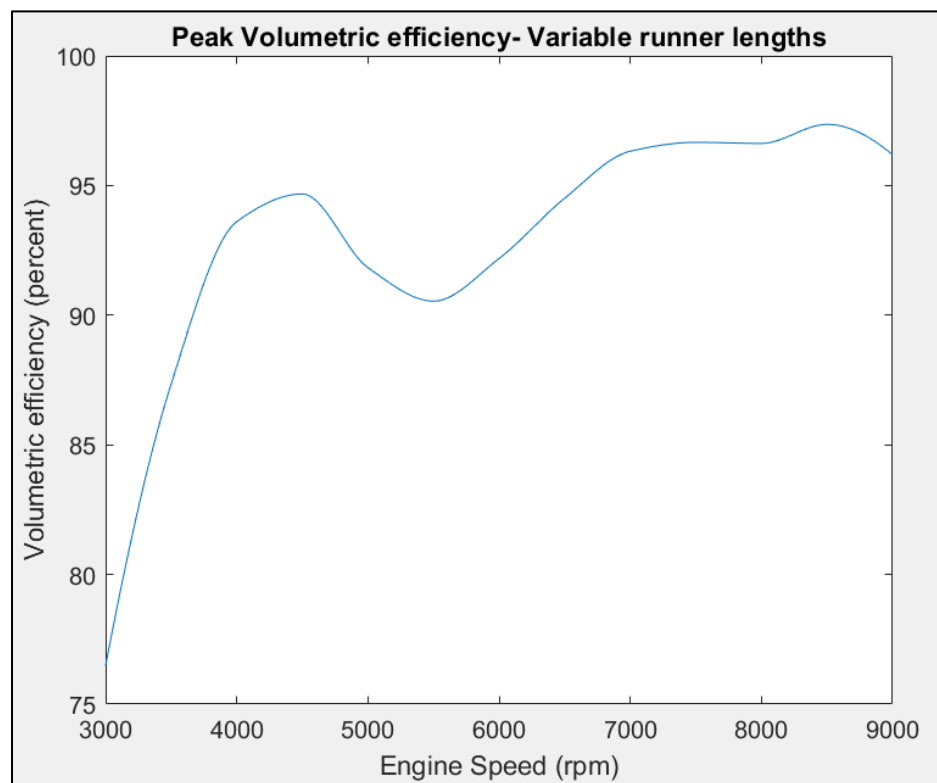


FIGURE 26: Peak volumetric efficiency with a multiple variations in runner lengths

To achieve the volumetric efficiency shown in Figure 26 an infinitely variable runner length set-up would be needed. As mentioned earlier, it is not so feasible to manufacture an infinitely variable runner set-up that has a high enough frequency response to match with that of the engine's speed variations. Hence, the engine speed range is divided in two groups and the best runner length was found for these two groups. The chosen runner lengths are shown in Figure 27. The resulting volumetric efficiency is compared with the stock volumetric efficiency and the maximum attainable volumetric efficiency by infinite runner length variations and is shown in Figure 28. It can also be seen from the Figure 27, that longer length runners favor performance at low engine speed ranges, whereas shorter runner favor performance at higher engine speeds.

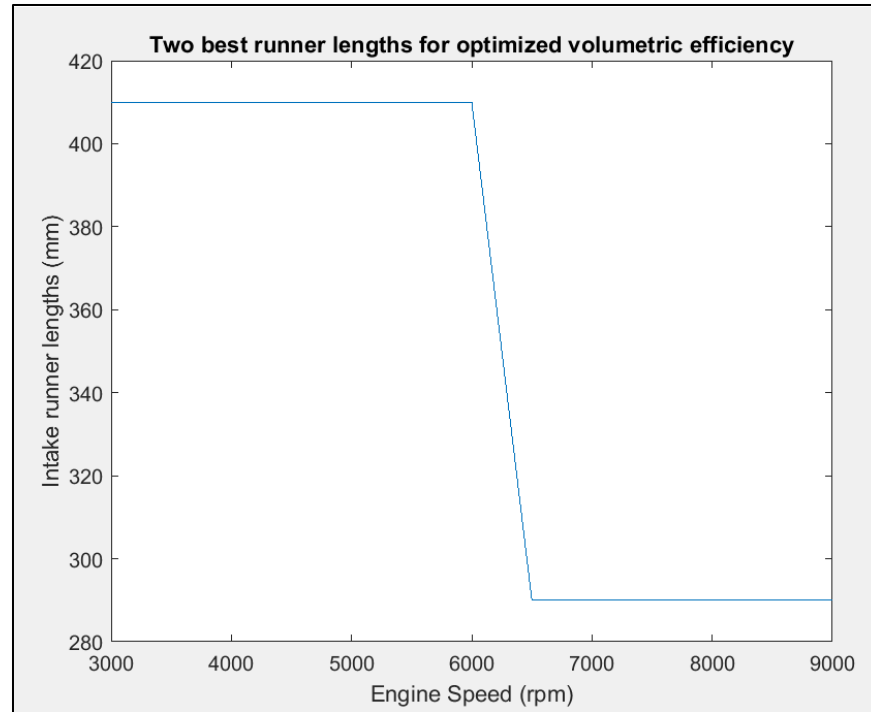


FIGURE 27: Two best runner lengths to optimize volumetric efficiency

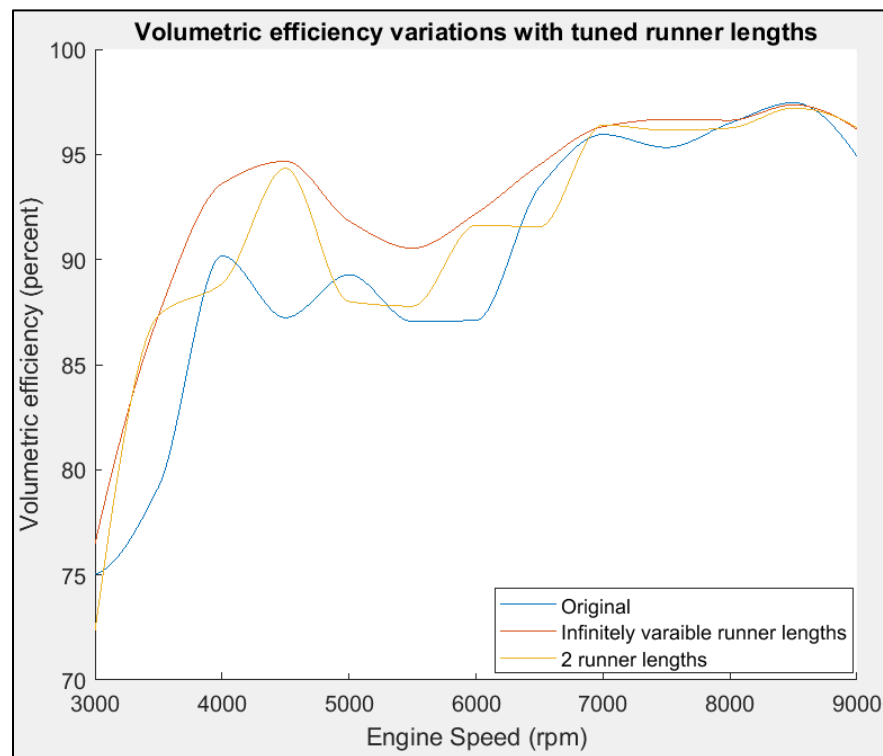


FIGURE 28: Comparison of volumetric efficiency (i) original runner length, (ii) infinitely variable runner lengths (iii) two runner lengths

TABLE 4: Volumetric efficiency variations with respect to (wrt) runner lengths

Engine Speed	Original	Infinitely variable lengths	% Increase wrt original	2 Variation in lengths	% Increase wrt original
3000	0.75	0.76	1.94	0.72	-3.59
3500	0.79	0.87	10.31	0.87	10.31
4000	0.90	0.94	3.80	0.89	-1.46
4500	0.87	0.95	8.52	0.94	8.14
5000	0.89	0.92	2.86	0.88	-1.43
5500	0.87	0.91	4.00	0.88	0.83
6000	0.87	0.92	5.83	0.92	5.20
6500	0.93	0.95	1.14	0.92	-2.02
7000	0.96	0.96	0.39	0.96	0.47
7500	0.95	0.97	1.40	0.96	0.86
8000	0.96	0.97	0.14	0.96	-0.24
8500	0.97	0.97	0.00	0.97	-0.26
9000	0.95	0.96	1.33	0.96	1.42

It can be seen from Figure 28 and Table 4 that the volumetric efficiency of the engine is boosted by an average of 3.2% throughout the engine speed range when infinitely variable runner lengths are used. When only 2 variations in runner length are used, the volumetric efficiency has boosted by an average of 1.4% throughout the engine speed range. But this boost came at the cost of reduction in volumetric efficiency at certain engine speeds. This is because the chosen runner lengths are not the best for those engine speeds. It is also known that engine volumetric efficiency is a function of valve opening time. Hence, to make up for these losses valve opening time will be varied along the engine operating speed range.

3.2: EFFECTS OF VARYING INTAKE VALVE TIMING

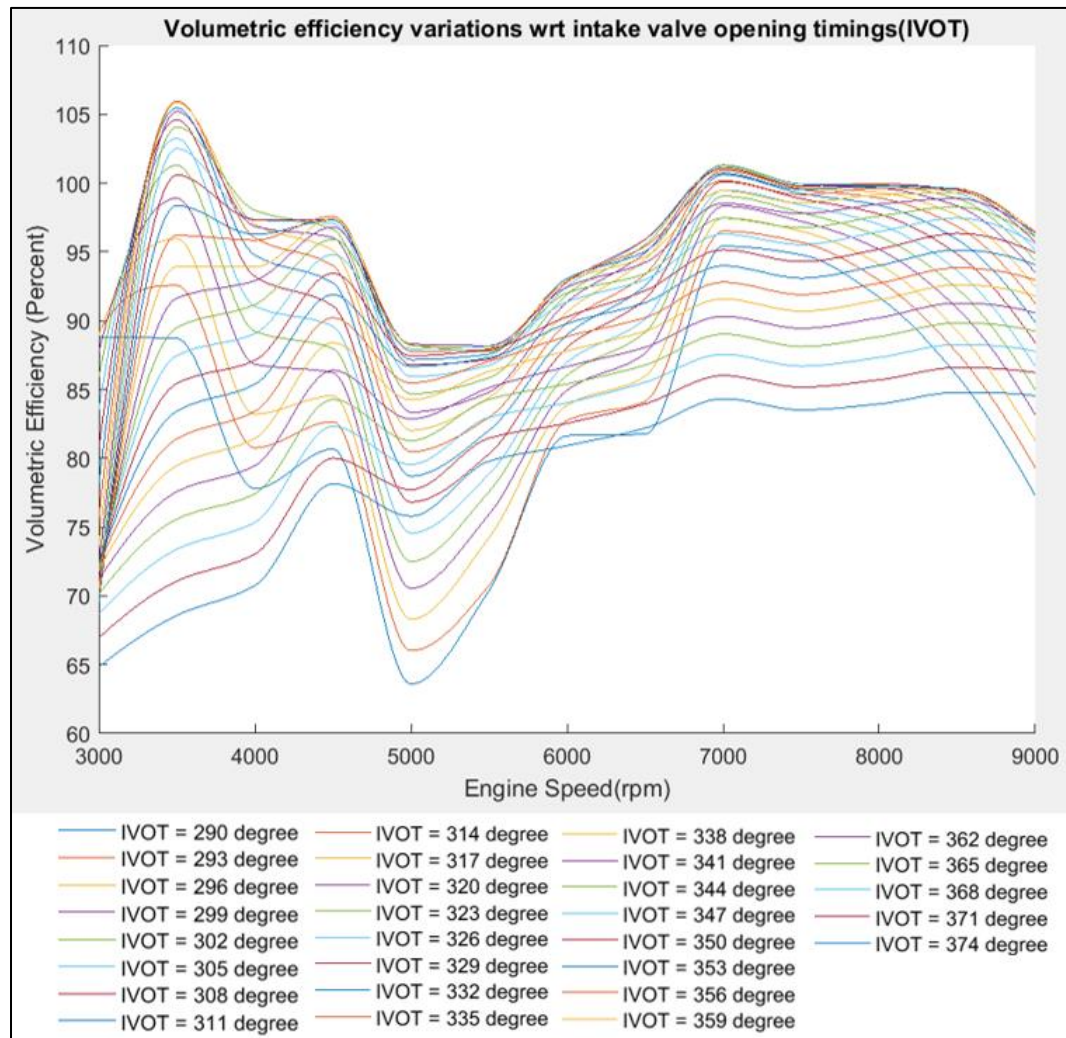


FIGURE 29: Variations in volumetric efficiency with respect to (wrt) intake valve opening timing

Figure 29 shows that volumetric efficiency is equally sensitive to valve opening timings as much as the intake runner lengths. It can also be seen from the above figure that the peak volumetric efficiencies at around 3500 rpm and 7000 rpm have increases above 100 %, thus supercharging the engine. Hence, it is evident that appropriate tuning can be used to supercharge the engines and that's why this technique is rightly known as acoustic supercharging.

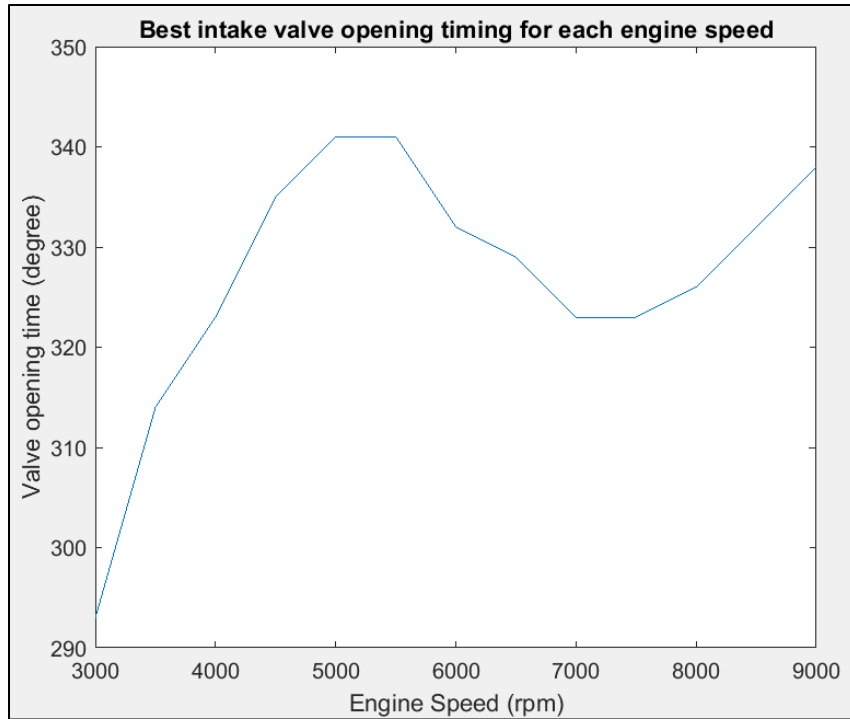


FIGURE 30: Best valve opening times for each engine speed

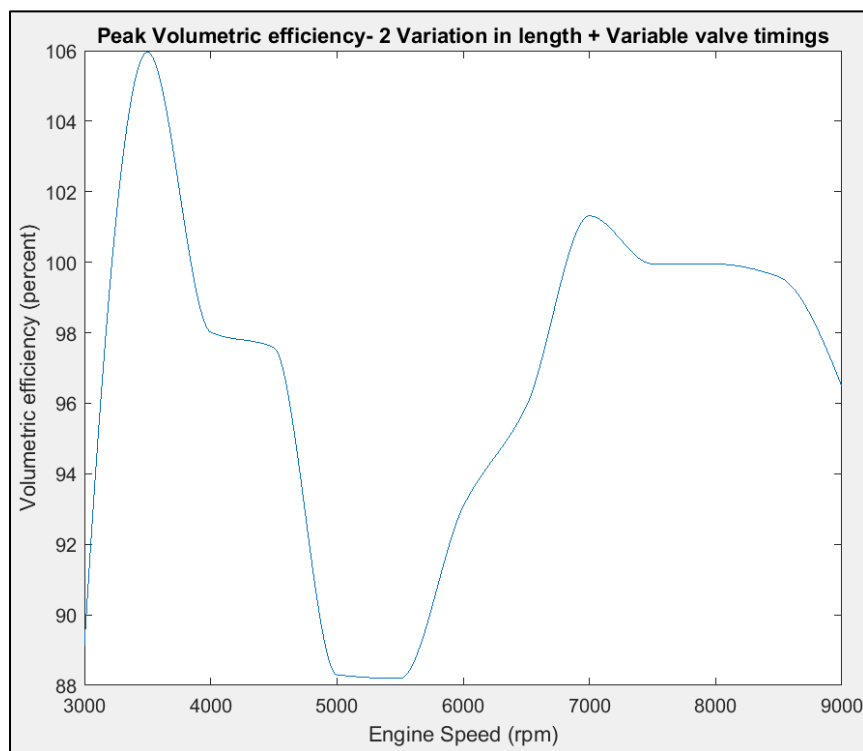


FIGURE 31: Peak volumetric efficiency with 2 variations in runner length and multiple variations in valve timing

The best valve opening timings for each speed simulated are shown in Figure 30. The peak attainable volumetric efficiency with a combination of 2 variations in runner lengths and infinitely variable valve opening timings would be the curve joining the peaks volumetric efficiency at each engine speed. The set of valve timings where this peak efficiency is attained is shown in Figure 30 and the resulting volumetric efficiency is shown in Figure 31.

Just like the intake runners, to manufacture a system that could change valve opening timings infinitely, would be complicated due to the high frequency response requirement to work in synchronization with the high speed of the engine. Hence, two variations of valve timing over two ranges of engine speeds that would provide optimum performance have been chosen. The two variations in valve timings that give the best result have been shown in Figure 32. It is evident that early opening of valves at lower speeds (higher overlap duration in degrees) and late opening (lower overlap duration in degrees) of valves at the higher speeds would be best to optimize the gas exchange process. The resulting volumetric efficiency is shown in Figure 33.

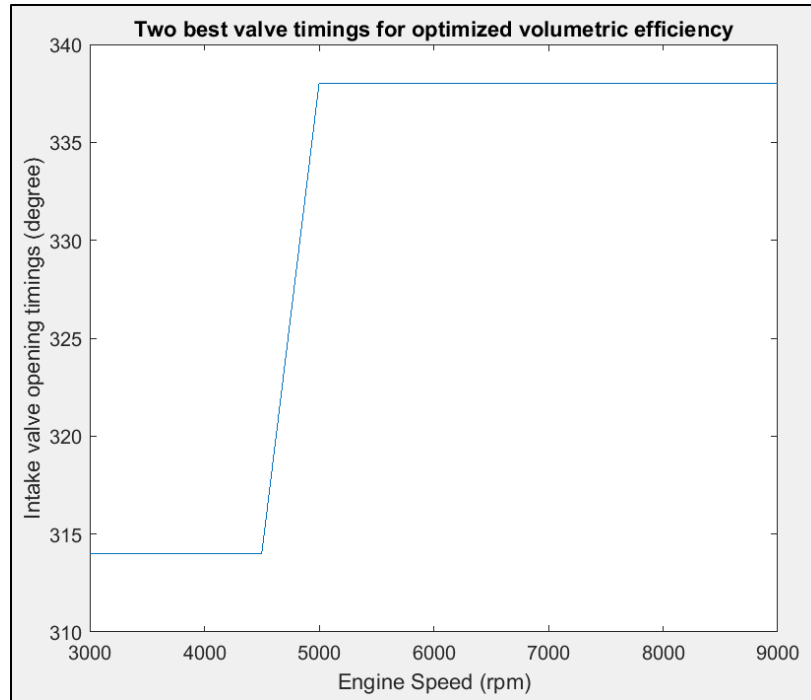


FIGURE 32: Two best valve opening timings along for optimized volumetric efficiency

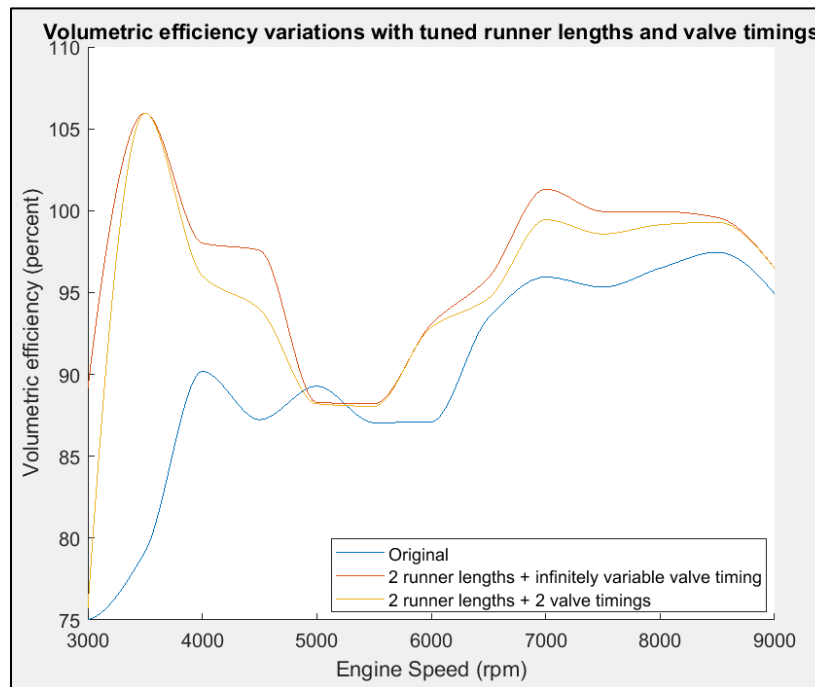


FIGURE 33: Comparison of volumetric efficiency- (i) original

(ii) 2 runner lengths + variable valve timings

(iii) 2 runner lengths + 2 valve opening timings

TABLE 5: Comparison of volumetric efficiency wrt variable valve timings

Engine Speed	Original	2 Lengths + variable valve timings	% Increase wrt original	2 Lengths + 2 valve timings	% Increase wrt original
3000	0.75	0.90	19.88	0.76	0.93
3500	0.79	1.06	34.43	1.06	33.82
4000	0.90	0.98	8.22	0.96	6.48
4500	0.87	0.98	12.34	0.94	7.75
5000	0.89	0.89	-0.84	0.88	-1.21
5500	0.87	0.88	0.87	0.88	1.15
6000	0.87	0.93	7.12	0.93	6.62
6500	0.93	0.94	0.46	0.95	1.28
7000	0.96	1.01	5.79	0.99	3.64
7500	0.95	1.00	5.18	0.99	3.40
8000	0.96	1.00	3.23	0.99	2.75
8500	0.97	0.99	1.91	0.99	1.89
9000	0.95	0.97	2.61	0.96	1.65

From Figure 33 and Table 5 the losses in volumetric efficiency at few engine speeds that are encountered in Figure 28 and Table 4 due to choosing only two variations of runner lengths are almost recovered at all engine speeds. Due to infinitely variable valve timings along with 2 variations in runner lengths, the volumetric efficiency has boosted by an average of 7.78 %. There is a huge improvement as compared to the 3.2 % encountered with infinitely variable runner lengths alone. Due to the existence of two different runner lengths, the span of variations required in valve timing is reduced, further optimizing the volumetric efficiency. However, to ensure feasibility of the design, manufacturing, assembly and operation, it is better to use only 2 valve timings. Figure 33 and Table 5 also show that with the co-presence of only 2 different runner lengths and 2 different valve opening timings, the average boost of 5.40 % in volumetric efficiency throughout the engine operating speed range is encountered.

3.3: EFFECTS OF VARIABLE INTAKE VALVE LIFT

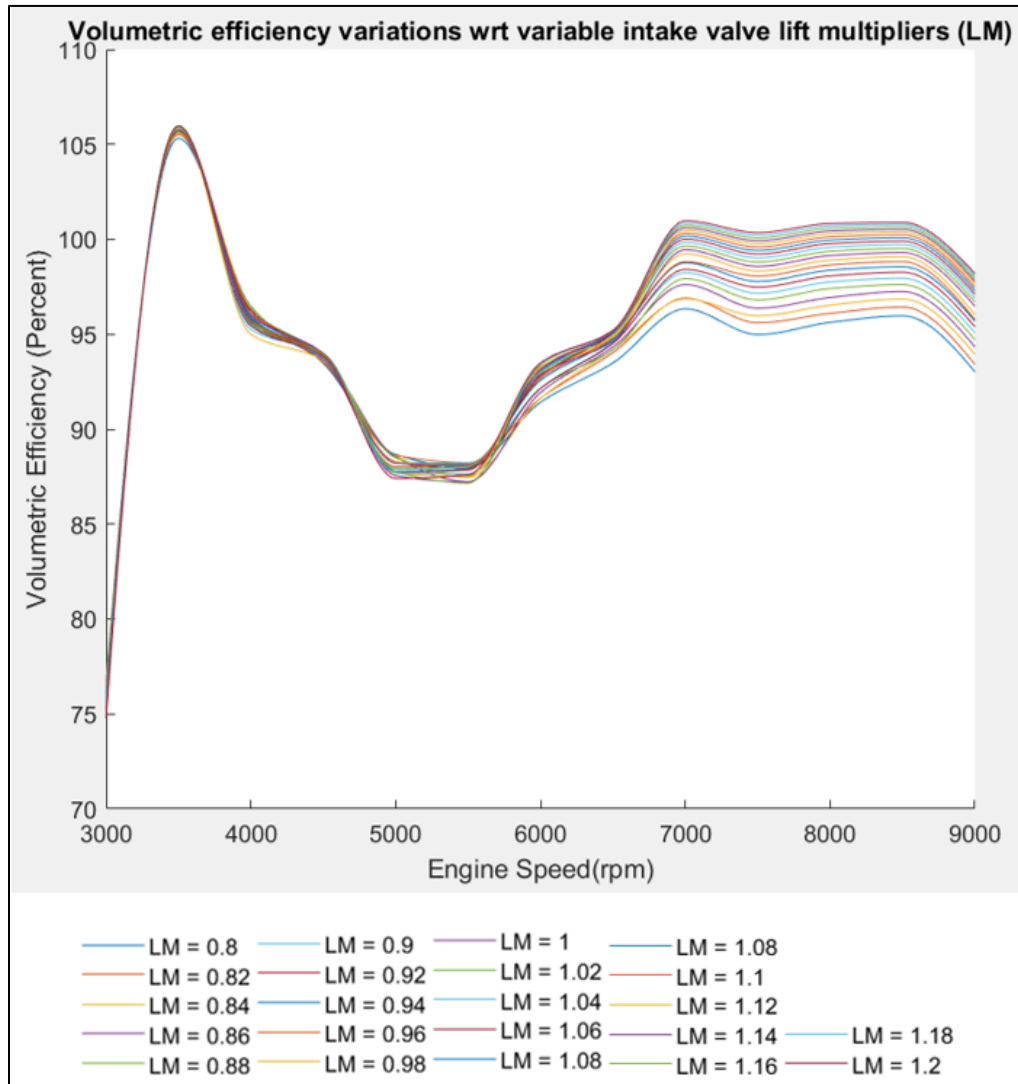


FIGURE 34: Volumetric efficiency variations with respect to (wrt) variable intake lift multipliers

To further increase the volumetric efficiency of the engine by more precise control over the induction pressure waves, the valve lifts are also varied. The valve lifts are varied by varying the valve lift multiplier from 0.8 to 1.2 in steps of 0.02. The original value of maximum valve lift is 9.7028 mm. The maximum lift is varied from 7.7622 mm to 11.6433 mm. The resulting variations in volumetric efficiency are shown in Figure 34.

Just like variable lengths and variable valve times, the engine performance is also sensitive to valve lifts. But, since it already has optimized runner lengths and valve timings, the engine performance is not seen to be as sensitive as it was to changes in runner lengths and valve timings. Again, the curve joining the peaks of volumetric efficiency at each simulated engine speed will give the most optimized engine performance. Figure 35 shows the valve timings corresponding to the peak volumetric efficiency at each engine speed simulated and Figure 36 shows the resultant volumetric efficiency.

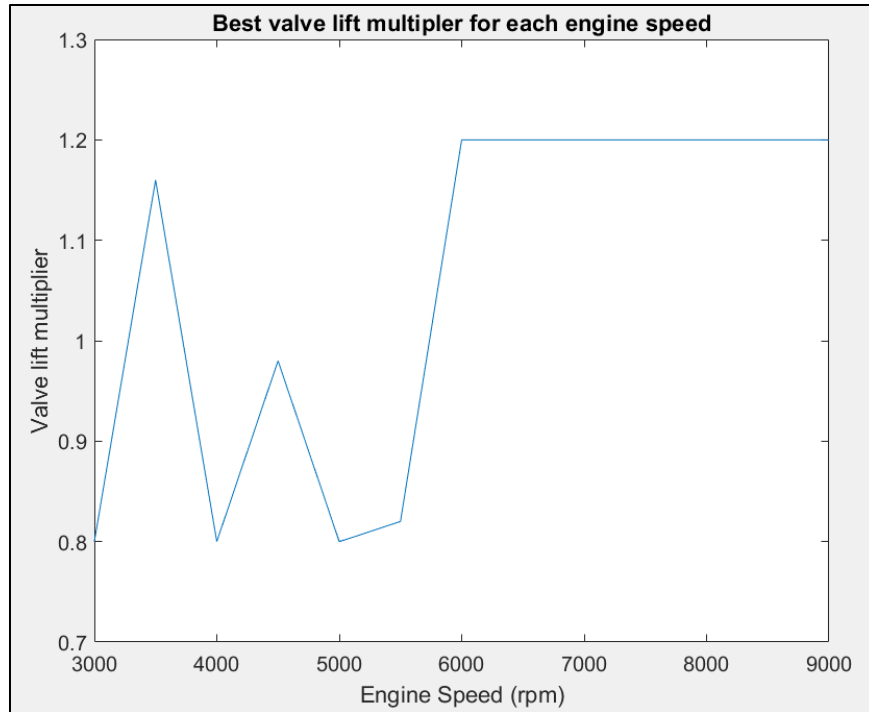


FIGURE 35: Best valve lift multipliers for each engine speed.

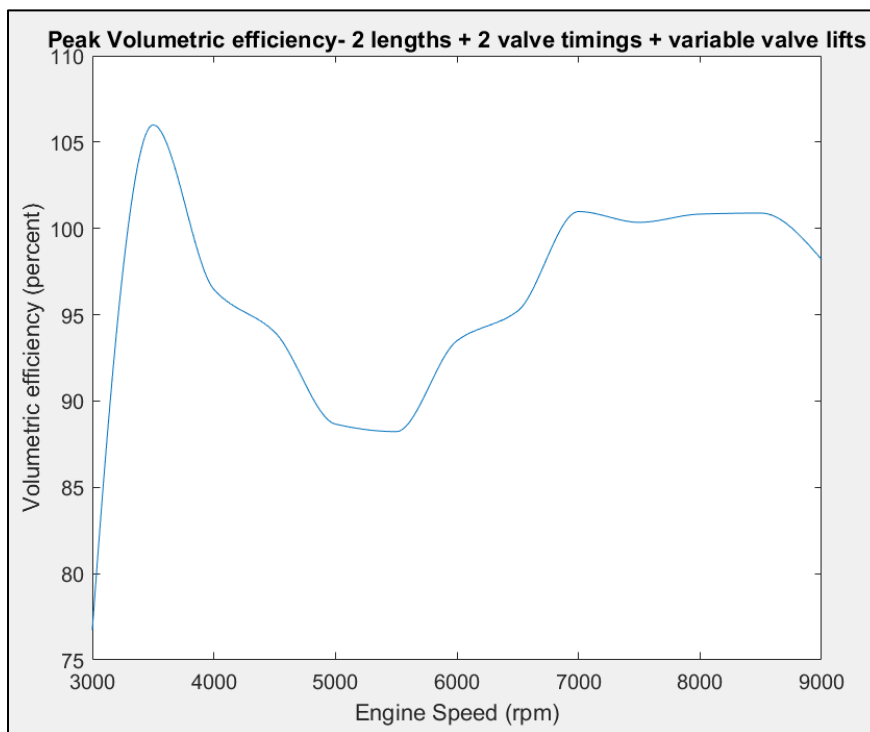


FIGURE 36: Peak volumetric efficiency with 2 variations in runner lengths and valve timings and multiple variations in valve lifts

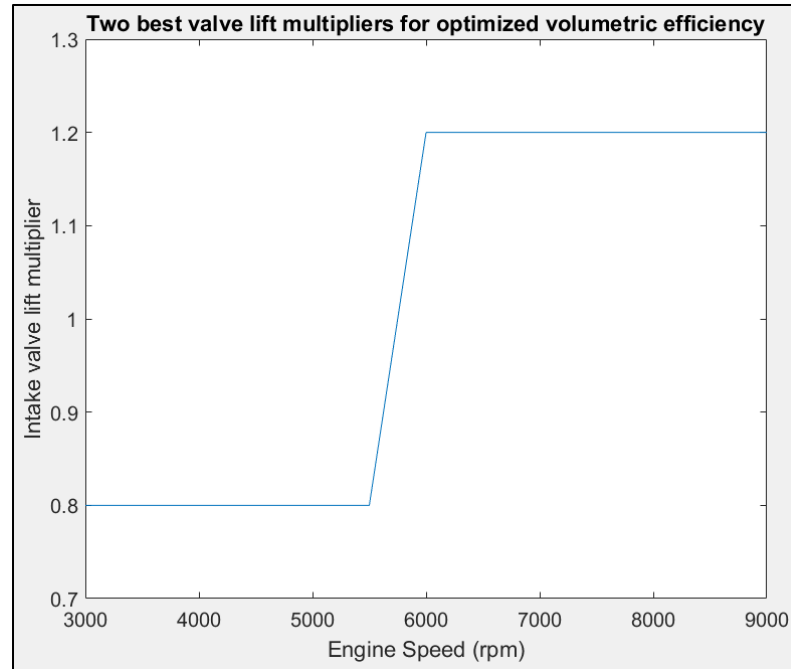


FIGURE 37: Two best valve opening timings along for optimized volumetric efficiency

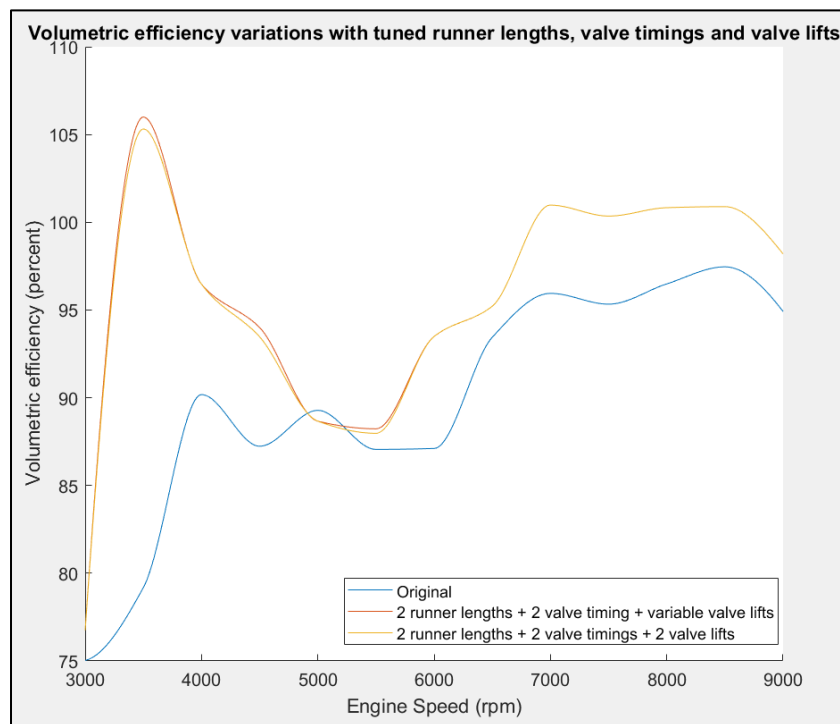


FIGURE 38: Comparison of volumetric efficiency- (i) original

(ii) 2 runner lengths + 2 valve timings + variable valve lifts

(iii) 2 runner lengths + 2 valve opening timings + 2 valve lifts

Like runner lengths and valve timings, two variations of valve lifts are also chosen to make the manufacturing and assembly of this concept more feasible. The two valve lift multipliers that gives the best results are shown in Figure 37. As mentioned earlier, reducing peak valve lift will benefit at lower engine speeds and increasing valve lift will benefit at higher engine speeds.

TABLE 6: Comparison of volumetric efficiency wrt variable valve lifts

Engine Speed	Original	Infinitely variable lengths	% Increase wrt original	2 Variation in lengths	% Increase wrt original
3000	0.75	0.77	2.28	0.77	2.28
3500	0.79	1.06	33.87	1.05	33.01
4000	0.90	0.96	6.98	0.96	6.98
4500	0.87	0.94	7.75	0.93	7.14
5000	0.89	0.89	-0.69	0.89	-0.69
5500	0.87	0.88	1.35	0.88	1.05
6000	0.87	0.93	7.33	0.93	7.33
6500	0.93	0.95	1.89	0.95	1.89
7000	0.96	1.01	5.24	1.01	5.24
7500	0.95	1.00	5.27	1.00	5.27
8000	0.96	1.01	4.50	1.01	4.50
8500	0.97	1.01	3.52	1.01	3.52
9000	0.95	0.98	3.46	0.98	3.46

Figure 38 shows the comparison of the volumetric efficiency with the stock (original) intake assembly, assembly with 2 variations in runner lengths, valve timings and valve lifts and the assembly with 2 variations in runner lengths and valve timings, but multiple variations in valve lifts. The engine performance has clearly improved in comparison to the original performance. The engine performance has improved by an average of 6.36 %. With limiting the valve lifts as well to only two variations of 7.76 mm and 11.64 mm, an average gain of 6.22% is achieved. Hence, there has been not been much

loss in the volumetric efficiency after due to limiting valve lift to only 2 variations. Also, the losses in volumetric efficiency have at 5000 rpm have reduced to 0.69%.

The volumetric efficiency at engine speeds of 3500, and 7000 to 9000 have boosted above 100% causing the engine to be supercharged at those speeds. Also, the average volumetric efficiency is now around 95%, which provides a relatively flat curve for volumetric efficiency. Hence, it can be said that the engine volumetric efficiency has been optimized by varying the runner lengths, valve timings and valve lifts almost fully just by two variations in each of them.

3.4: INDUCTION PRESSURE WAVES

The main reason for the optimization of the volumetric efficiency is the precise control on the induction pressure waves at each engine speed. As we keep varying more parameters in the induction assembly, the control on the induction pressure waves increases. Figures 39-42 show the induction pressure waves along with the corresponding valve profiles. If the induction waves are closely observed, the control on the pressure waves goes on increasing with every new parameter in the induction assembly being varied. The pressure waves in Figure 39, for the engine with the original induction system, are clearly not in synchronization with the valve opening timing. Rather than capturing the high-pressure waves, the intake valve opens when a low-pressure wave is present behind the intake valve.

When the intake runner lengths are tuned, as seen in Figure 40, the high-pressure wave arrives behind the intake valve before the valve opens. Also, another high-pressure wave can be seen occurring before the intake valve closes, suggesting that we are also taking advantage of the ramming effect of the air in the intake runner.

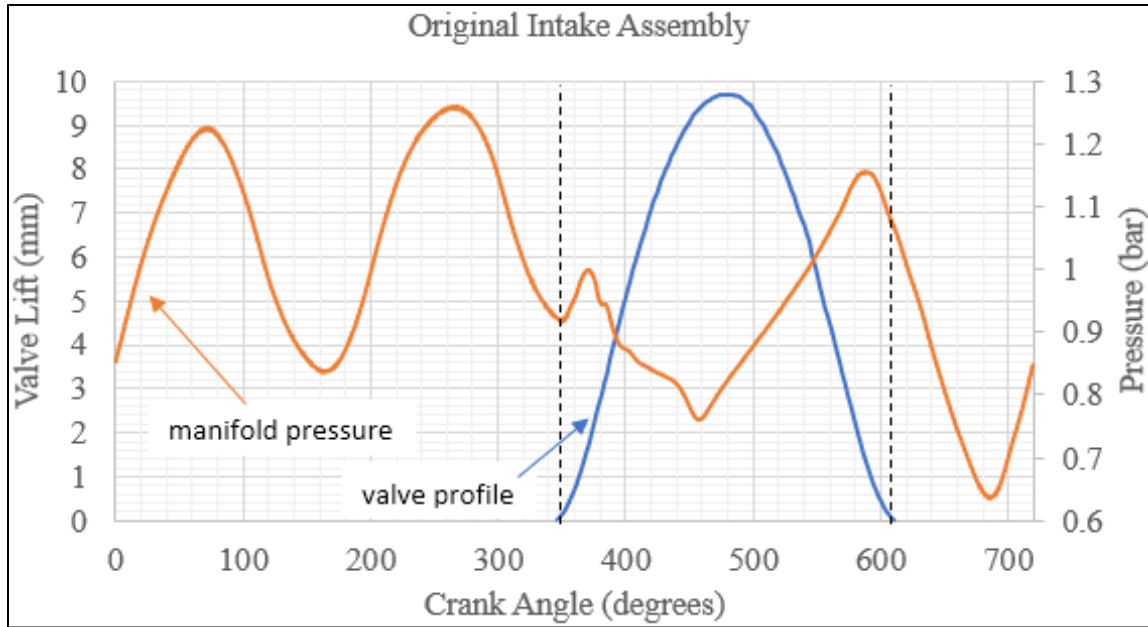


FIGURE 39: Comparison of valve profile and pressure waves for the case with original intake assembly at 6000 rpm

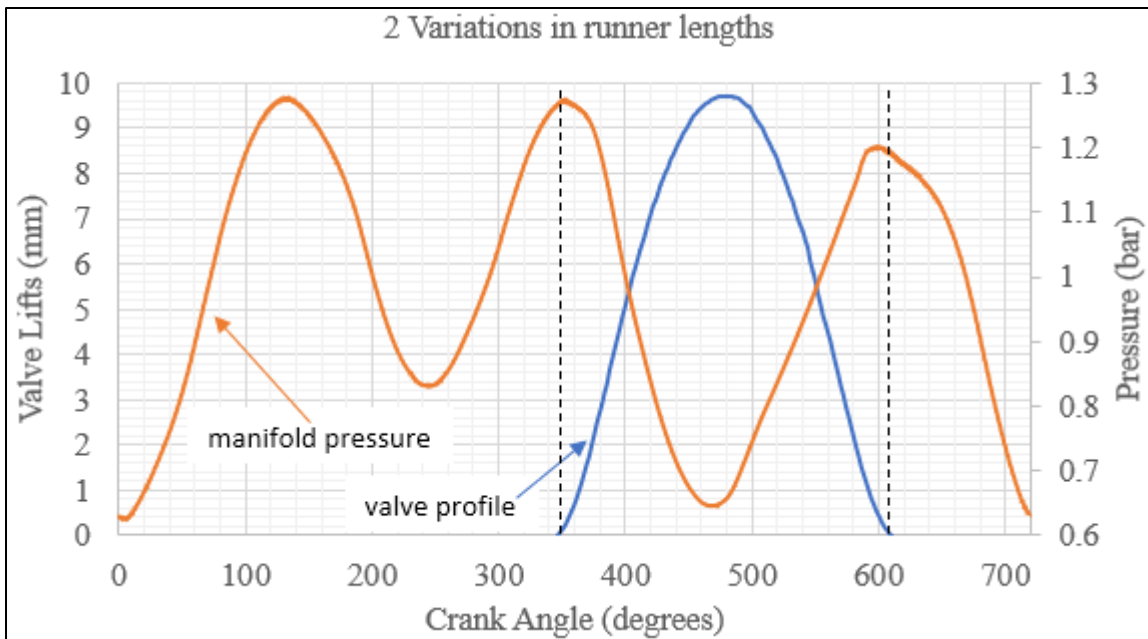


FIGURE 40: Comparison of valve profile and pressure waves for the case with 2 variations in runner lengths at 6000 rpm

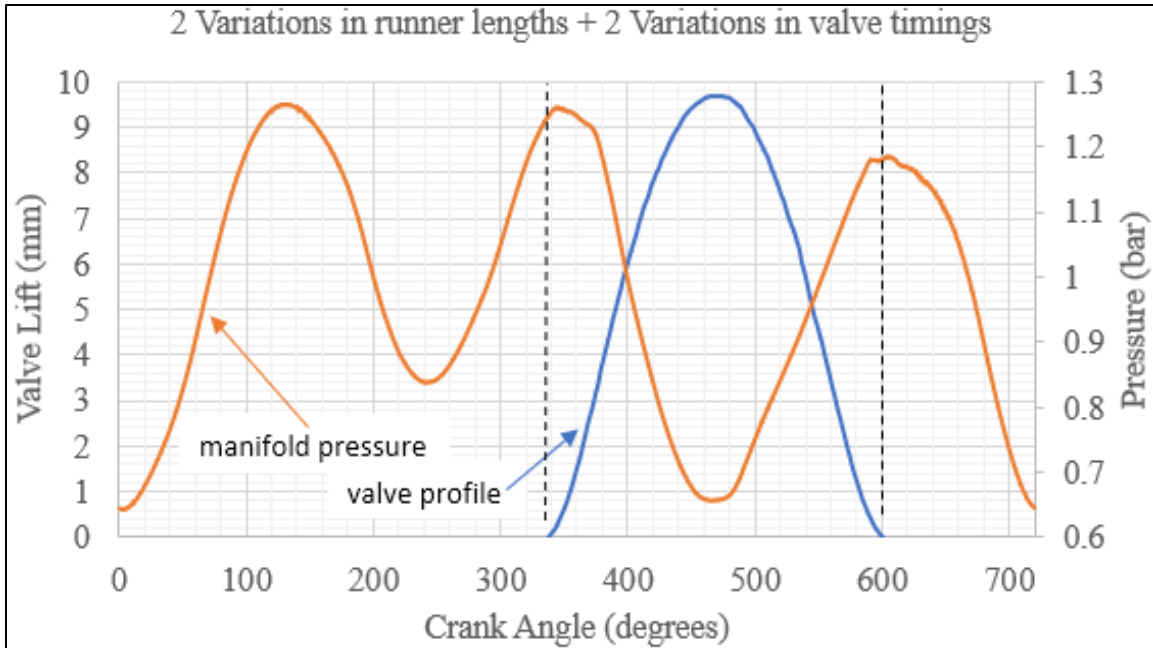


FIGURE 41: Comparison of valve profile and pressure waves for the case with original intake assembly at 6000 rpm

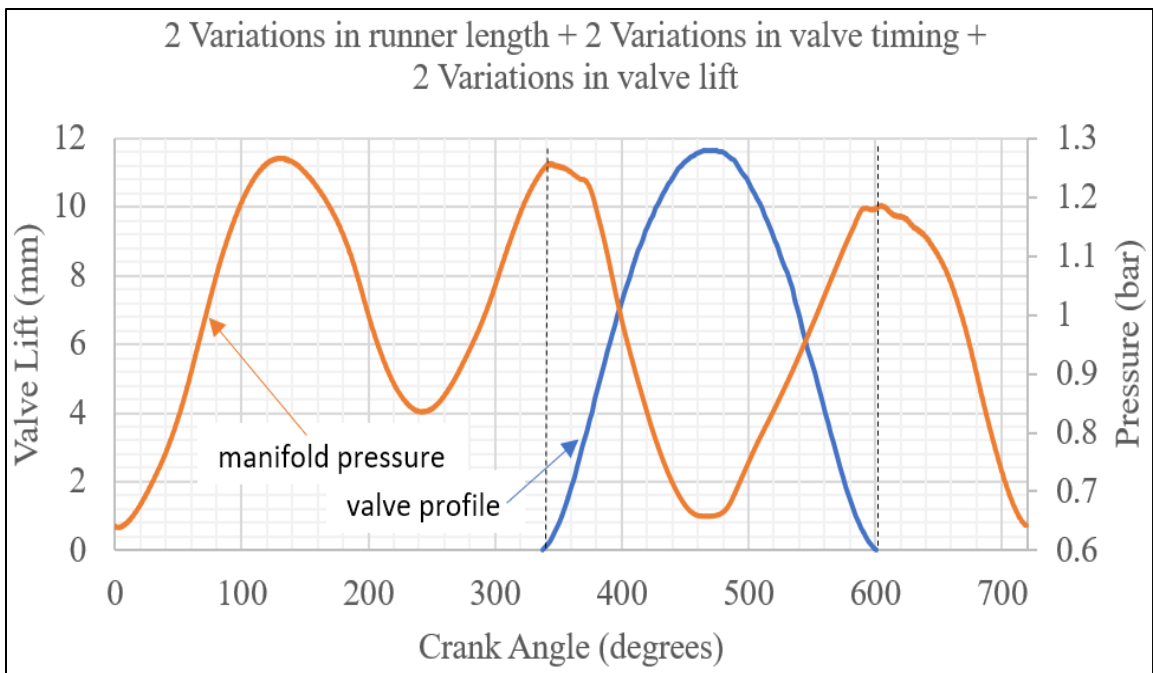


FIGURE 42: Comparison of valve profile and pressure waves for the case with original intake assembly at 6000 rpm

When the valve timings are changed at 7500 rpm, the induction pressure waves can be controlled more precisely. The amplitude of the induction pressure wave remains almost unchanged since the effective time when the intake valve is closed, and the pressure waves can travel back and forth along the intake manifold remains the same. However, with change in valve opening timings, the wave is controlled even better, and the intake valve is opened exactly when the peak of the pressure wave arrives, allowing to take the full advantage of the wave phenomenon.

Generally, for maximum volumetric efficiency at a given speed, lift should be kept as high as possible up to the point where the intake of fresh charge becomes restricted. The higher valve lift would provide more area for the flow of air from the manifold to the combustion chamber. Along with this, increasing valve lift is also seen to further fine tune the induction pressure wave and get it in synchronization with respect to the valve opening timing as seen in Figure 42.

3.5: EFFECTS ON POWER AND TORQUE PERFORMANCE

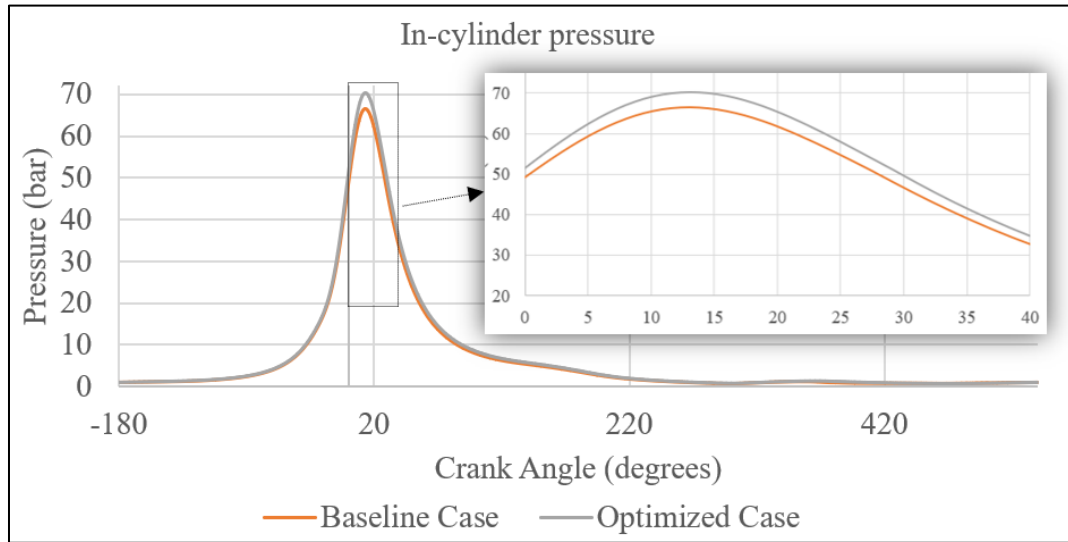


FIGURE 43: Comparison of in-cylinder pressures for 6000 rpm

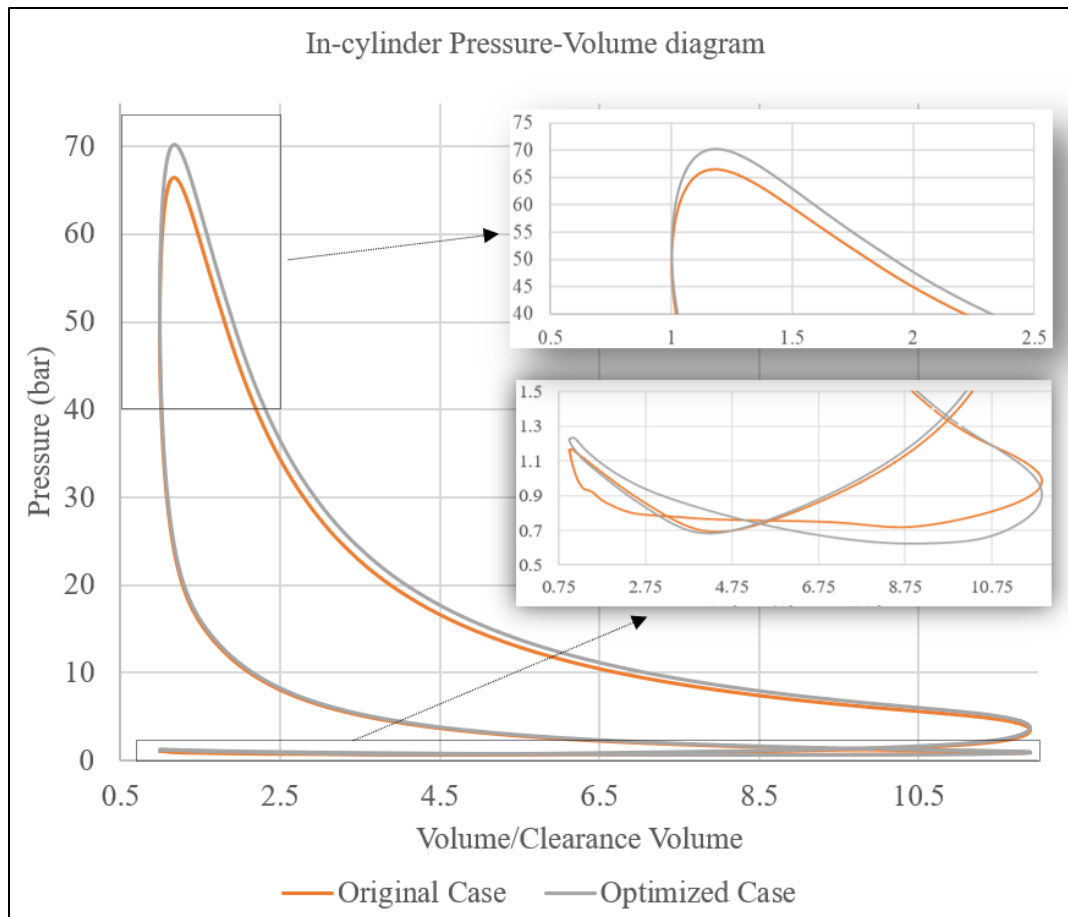


FIGURE 44: Comparison of pressure volume diagrams for 6000 rpm

With increase in the induction pressures as seen in Figure 43, the amount of air entering the combustion chamber increases. When the piston is at BDC and the intake valve is almost about to be shut, the air trapped inside the combustion chamber increases. This increases the pressure inside the combustion chamber. Now when the piston has travelled the stroke length and almost reached TDC, the pressure post compression is also higher as compared to the original engine. The peak cycle pressure increases from 66.5 bar to 70.3 bar. This can be seen in the Pressure-Volume (PV) diagram in Figure 44. Due to this the pressure post ignition is also higher than original. Hence, more force will be exerted on the piston moving towards BDC and thus the engine torque increases.

The area under the pressure-volume (PV) curve for a certain engine speed determines the power produced by the engine at that engine speed. Since the peak cycle pressure has increased, the area under PV curve has increased increasing the power produced.

The area under the part of the PV curve that represents the suction stroke shows the pumping losses. The pumping power is spent to perform the intake and exhaust strokes. With the tuned valve timings and increased valve lifts, the restrictions that the engine must overcome in the intake and exhaust strokes are reduced considerably, thus reducing the pumping losses as can be seen from the zoomed part of Figure 44. This increases the net brake horse power.

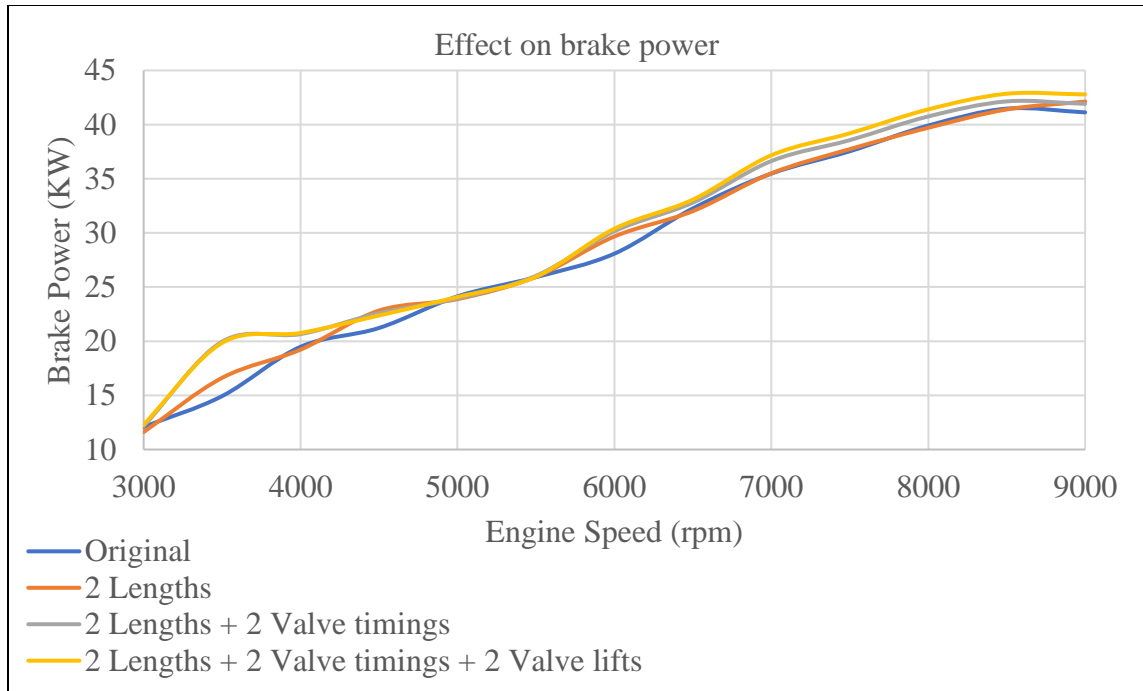


FIGURE 45: Comparison of maximum achievable brake power

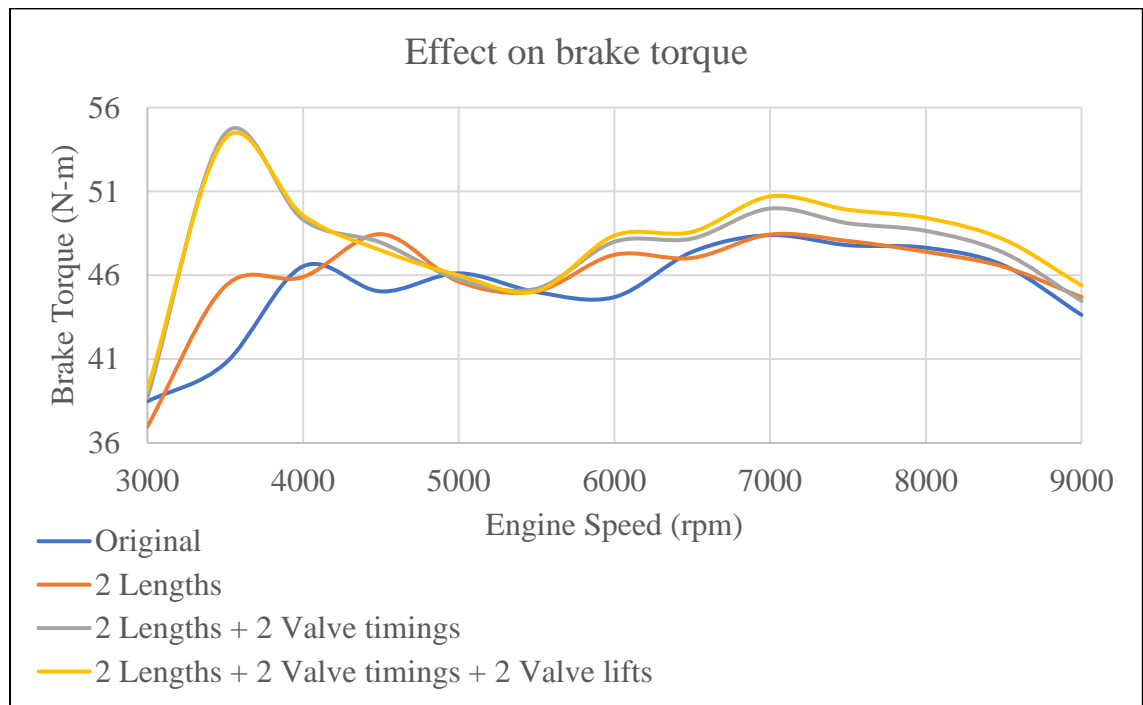


FIGURE 46: Comparison of maximum achievable brake torque

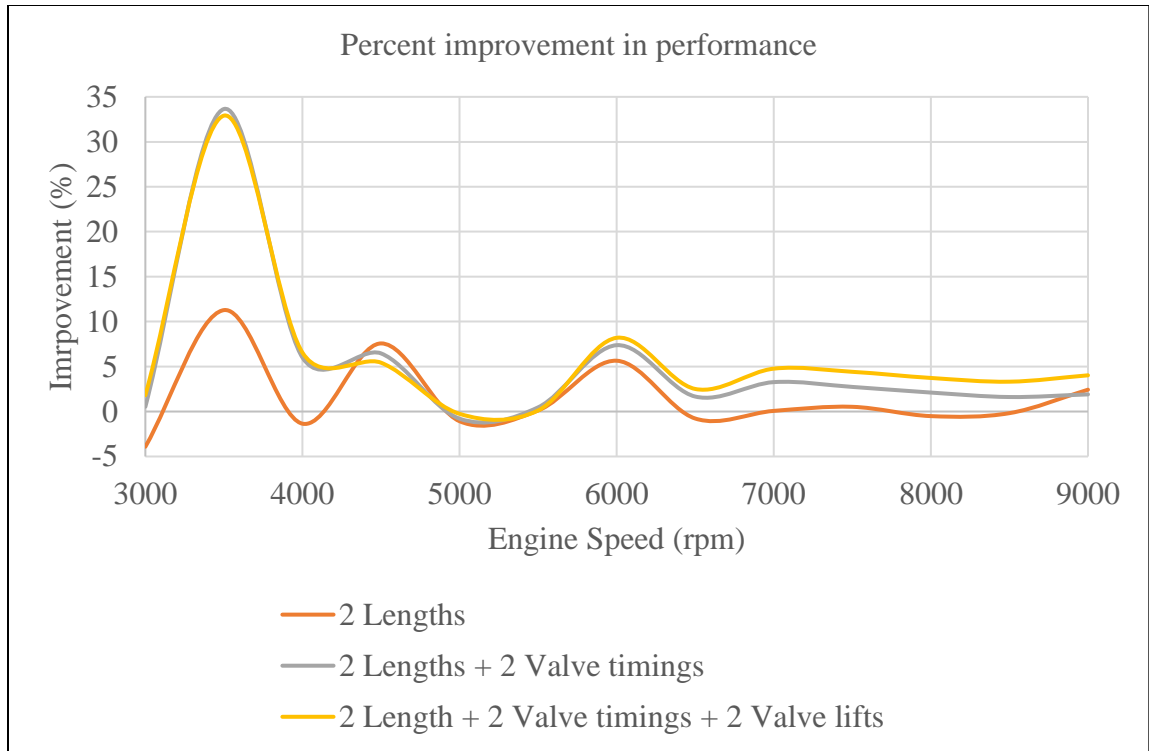


FIGURE 47: Comparison of maximum achievable brake torque

Figure 45-46 show the increase in power and torque performance of the engine. Like volumetric efficiency, torque and power increase with every new variation in the intake manifold parameters introduced. This increases the air induction pressure and thus the engine's overall performance. Figure 47 summarizes the improvements in power and torque performance of the engine. At low revving speeds of 3000 – 5000 rpm, an average improvement of 9.28% is encountered. At mid-range revving speeds of 5000-7000 rpm, an average improvement of 4% is encountered. At the high revving speeds of 7000-9000 rpm, an improvement of 3.87% is encountered. An average increase of 5.96% is seen throughout the engine operating speed range.

3.6: EFFECTS ON SPECIFIC FUEL CONSUMPTION

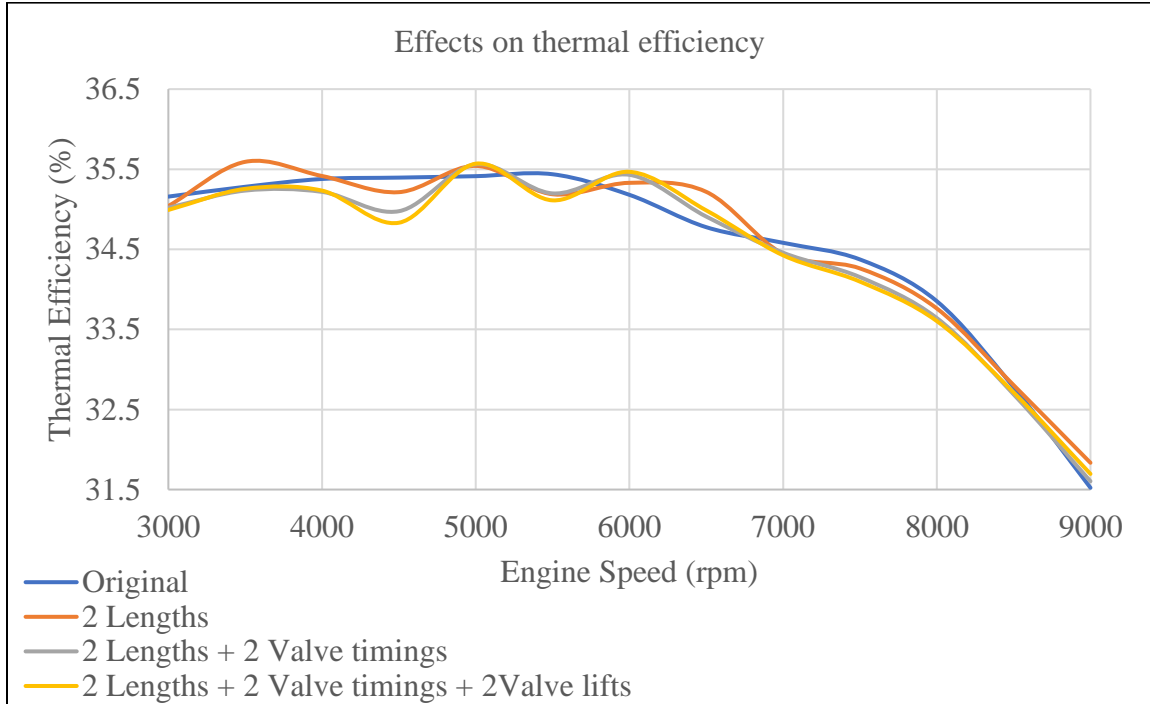


FIGURE 48: Comparison of thermal efficiency for various cases

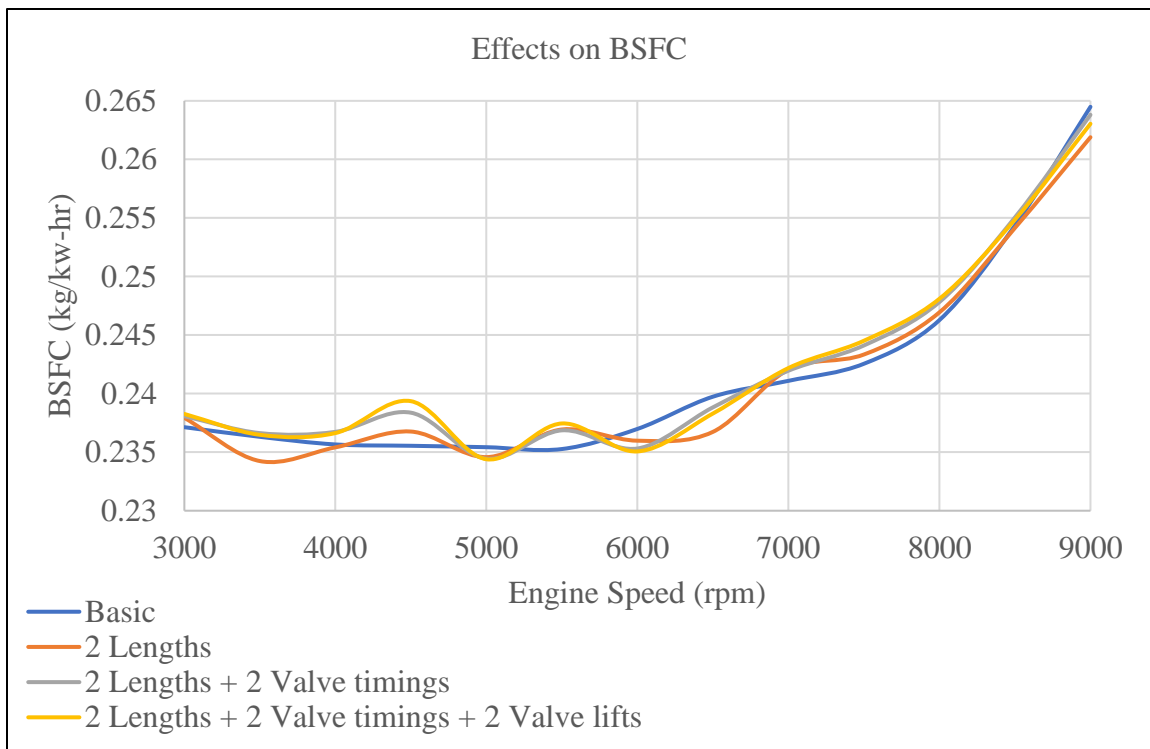


FIGURE 49: Comparison of thermal efficiency for various cases

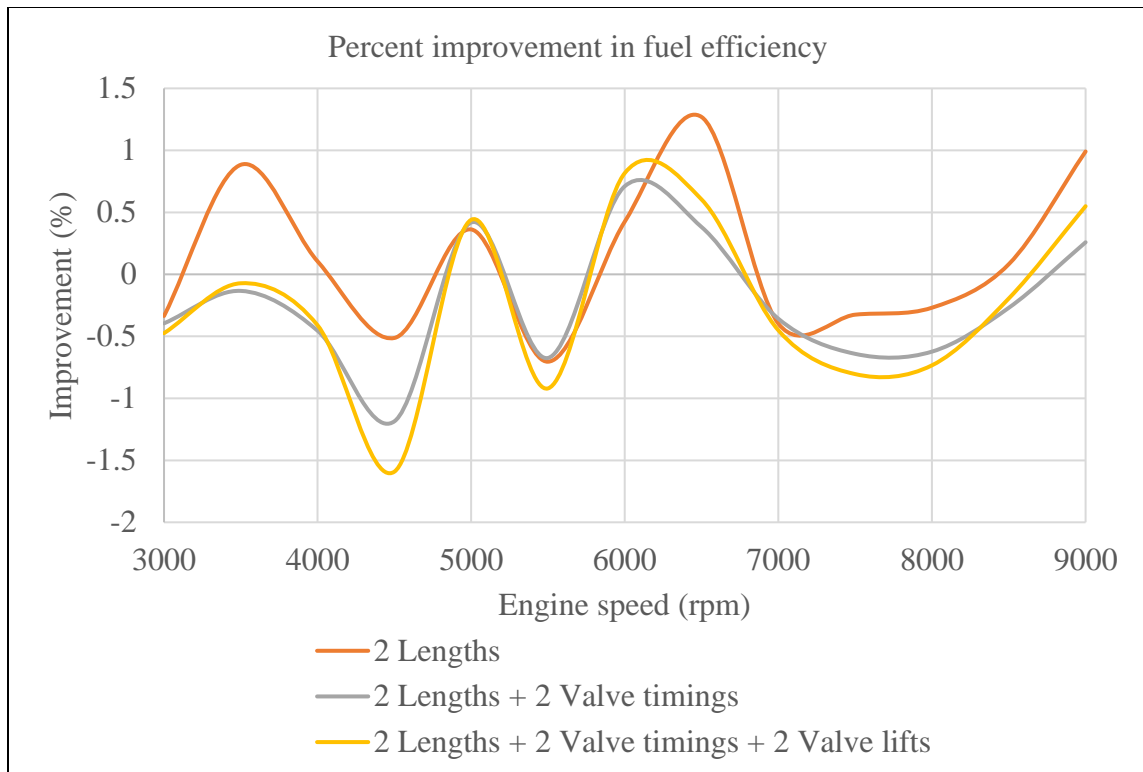


FIGURE 50: Comparison of thermal efficiency for various cases

Figure 47 shows the comparison of thermal efficiency of the engine for various cases simulated and Figure 48 shows the corresponding changes in brake specific fuel consumption. Even though the volumetric efficiency and the performance of the engine has increased with the change in runner lengths, valve timings and valve lifts, the thermal efficiency of the engine has not changed much, rather it has decreased by 0.24% on an average throughout the engine's operating speed range. This can be seen from Figure 50 which summarizes the effects of variable induction manifold on the fuel efficiency of the engine. This is because, the engine power has increased, but at the same time the fuel consumption has increased. The result is very useful for the motorsports industry where increasing power is the priority, but the need of the hour for the light motor vehicle industry is to reduce the fuel consumption even if the power and torque output is maintained at its current level of performance.

3.5: VARIATIONS IN AIR-FUEL RATIO

The modern trend in the automotive industry is to supercharge and undersize the engine to maintain the same engine performance and reduce the fuel consumption. To make up for these losses in fuel efficiency rather than increasing the vehicle performance, the engine's performance is simulated for leaner fuel-air mixtures.

The series of air-fuel ratios for which the simulated engine performance is found to be match the baseline engine performance are shown in Figure 51. As expected the engine can be now run on leaner air-fuel ratios if the stock performance of the engine is desired.

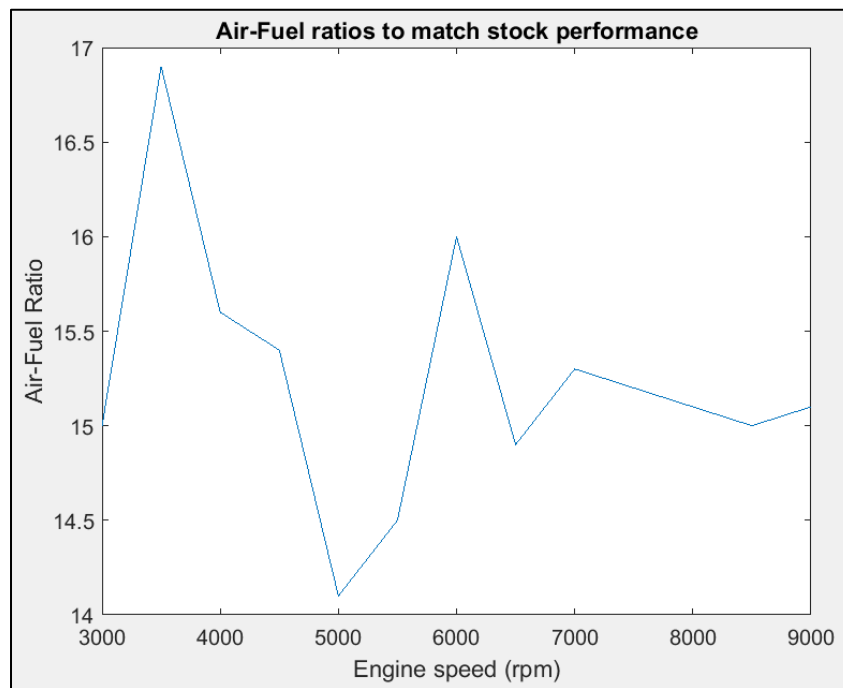


FIGURE 51: Air-Fuel ratios to match stock engine performance

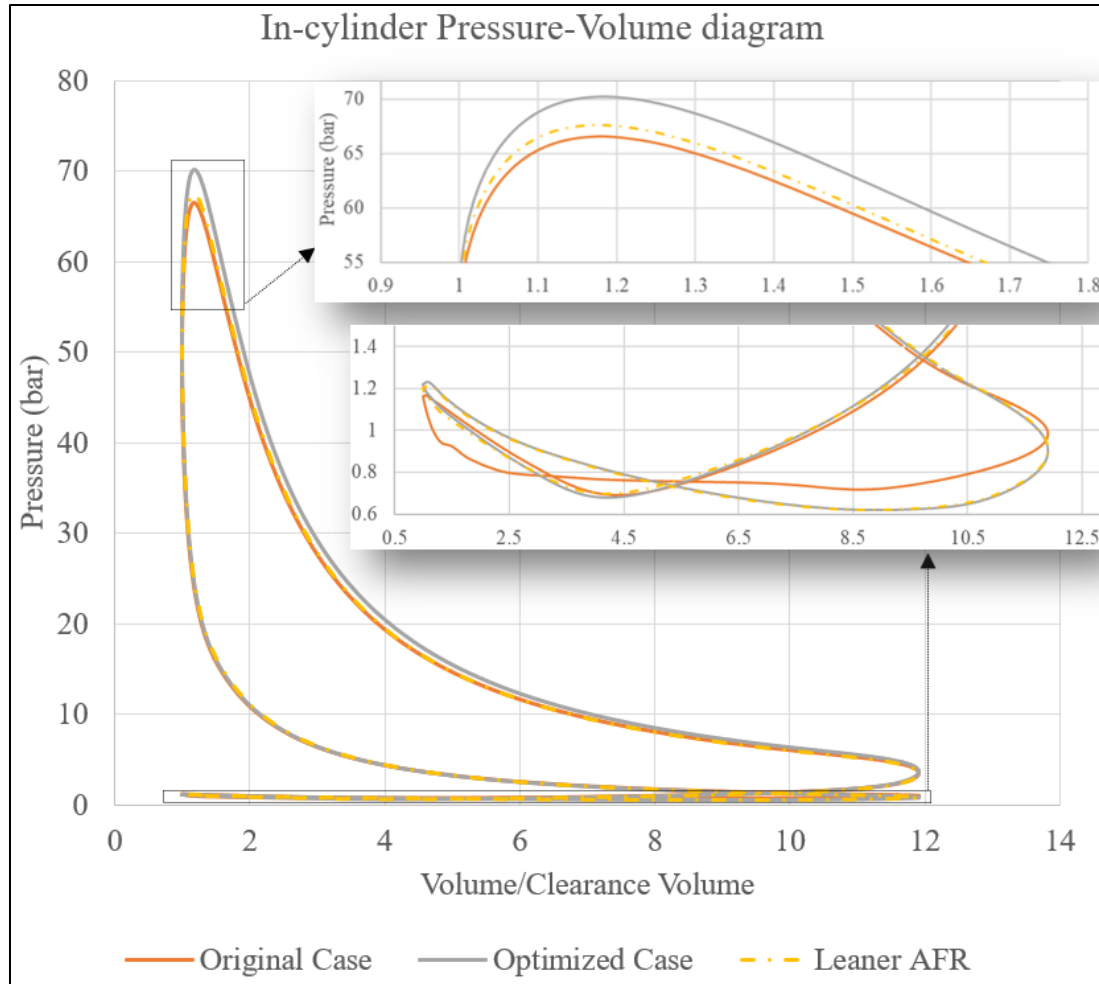


FIGURE 52: Comparison of pressure-volume diagram at 6000 rpm

Figure 52 compares the pressure-volume profiles of the stock engine, the engine with optimized intake assembly and the engine with optimized assembly operating on variable air-fuel ratios (AFR). By doing this, the peak cycle pressure post combustion is brought down close to that of the original cycle. The peak cycle pressure is brought down from 70.3 bar to 67.5 bar. The peak cycle pressure for the original cycle is 66.5 bar. Since the area under the pressure volume diagram is decreased, the engine power output has also decreased. At the same time, it can also be seen from Figure 52, that pumping loop for the optimized case before and after varying the air-fuel ratios is almost unchanged. Hence the gain in net brake power because of reduction in pumping losses is still the same.

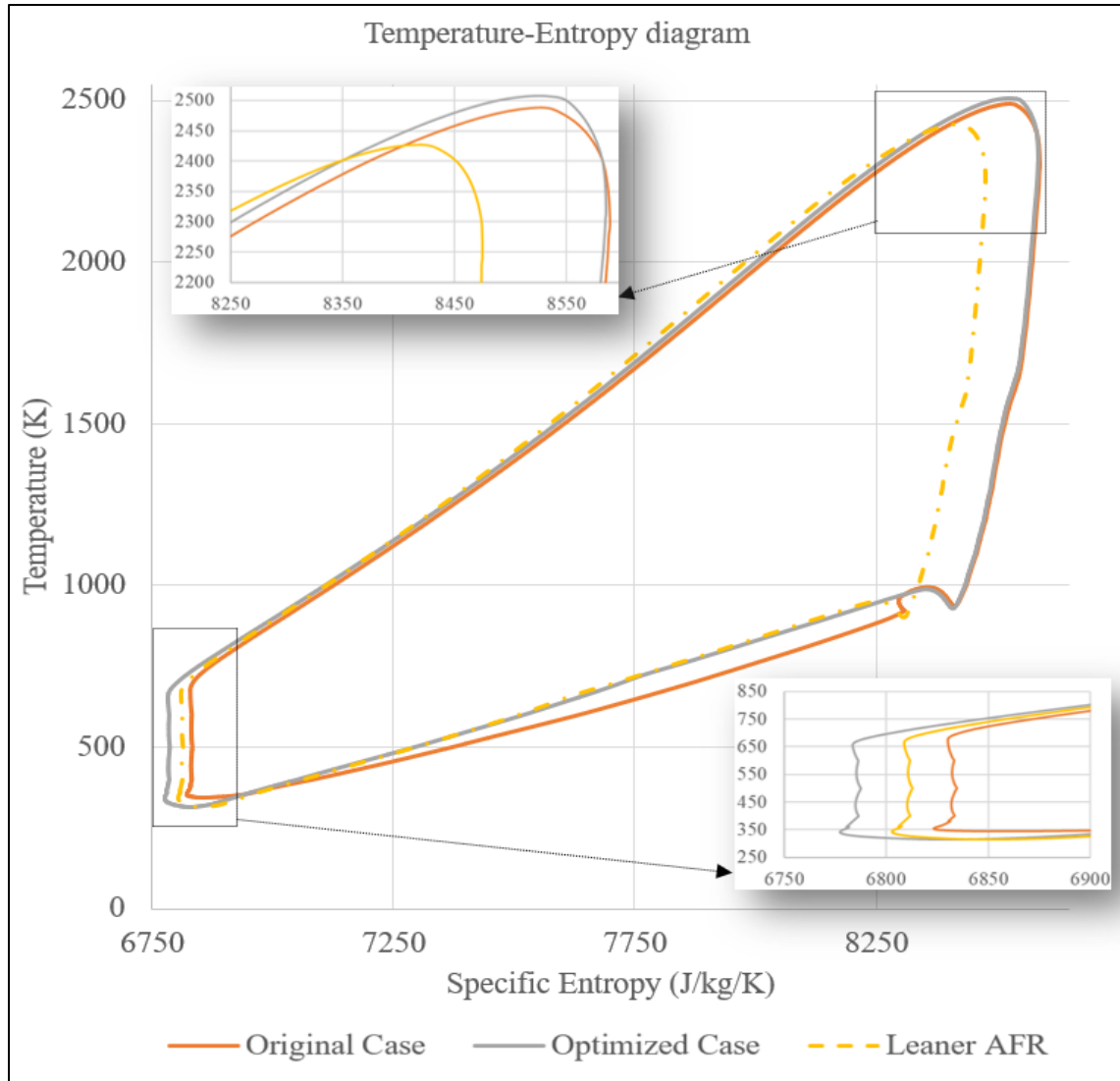


FIGURE 53: Comparison of temperature-entropy diagram at 6000 rpm

Figure 53 shows the comparison of the temperature vs specific entropy diagram for the original case, the optimized case with a constant air-fuel ratio and with a variable air fuel ratio at 6000 rpm. With the increase in peak cycle pressure, the peak cycle temperature has also increased from 2488 K to 2507 K. The cycle temperature after the power stroke is still almost the same. It is 930 K for the original case, while it is 934 K for the optimized case. Due to this reason the net power produced during this stroke has increased. Also, it can be clearly seen that the temperature after the intake stroke and just when the

compression stroke begins, is lower for the optimized case i.e. 336 K as compared to the original case i.e. 352 K. Also, the temperature post compression stage for the optimized case is 666 K whereas for the original case it is 691 K. This shows that the work input to the system for pumping has also decreased, thereby increasing the net work output. Since the net work output has increased (power stroke) and the net work input (compression stroke) has decreased, the net brake power produced by the engine has increased.

However, as an effect of the above, the heat supplied to the system (combustion chamber) has also increased, and hence the fuel consumption per unit power produced (BSFC). To tackle with this issue, when the air-fuel ratio is made leaner to match the engine's original performance, the peak cycle temperature drastically reduced to 2426 K. As can be seen from Figure 53, the heat supplied to the engine drastically reduced. However, the temperature before and after the compression stroke is still the same as the optimized case. This shows that we have still retained the power boost created by reducing the work input during compression stroke. Since the heat input to the system is now reduced considerably, the fuel consumption per unit power produced (BSFC) will also reduce considerably. The heat rejected during the exhaust stroke has also reduced. This will also further simplify the design for the cooling systems for the engine. The cooling system design being out of the scope of this research, has not been discussed about in detail. The resulting changes in the brake specific fuel consumption (BSFC) and the thermal efficiency of the engine are shown in Figure 54-55.

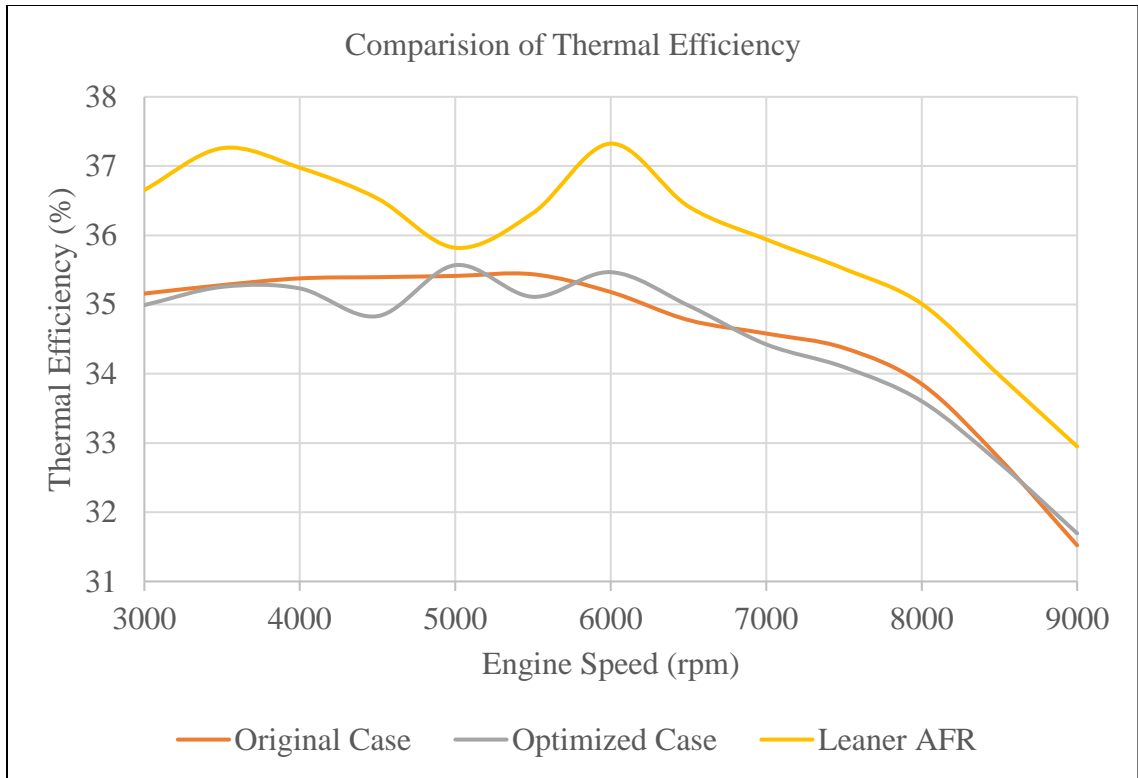


FIGURE 54: Comparison of thermal efficiency

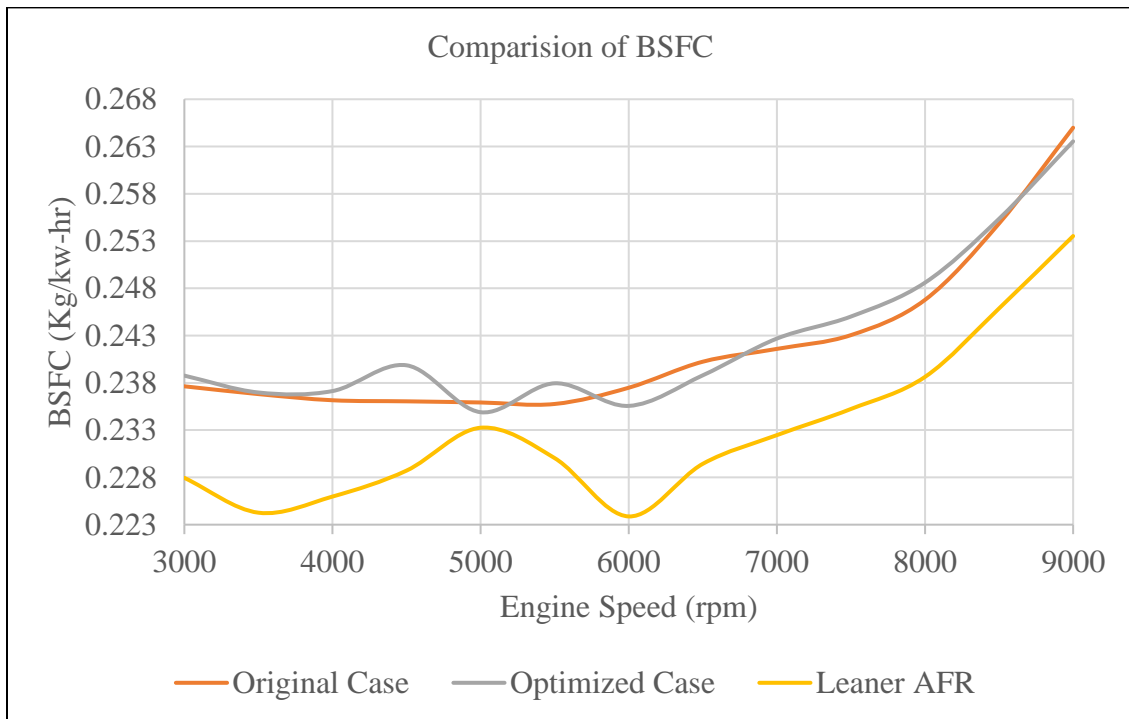


FIGURE 55: Comparison of BSFC

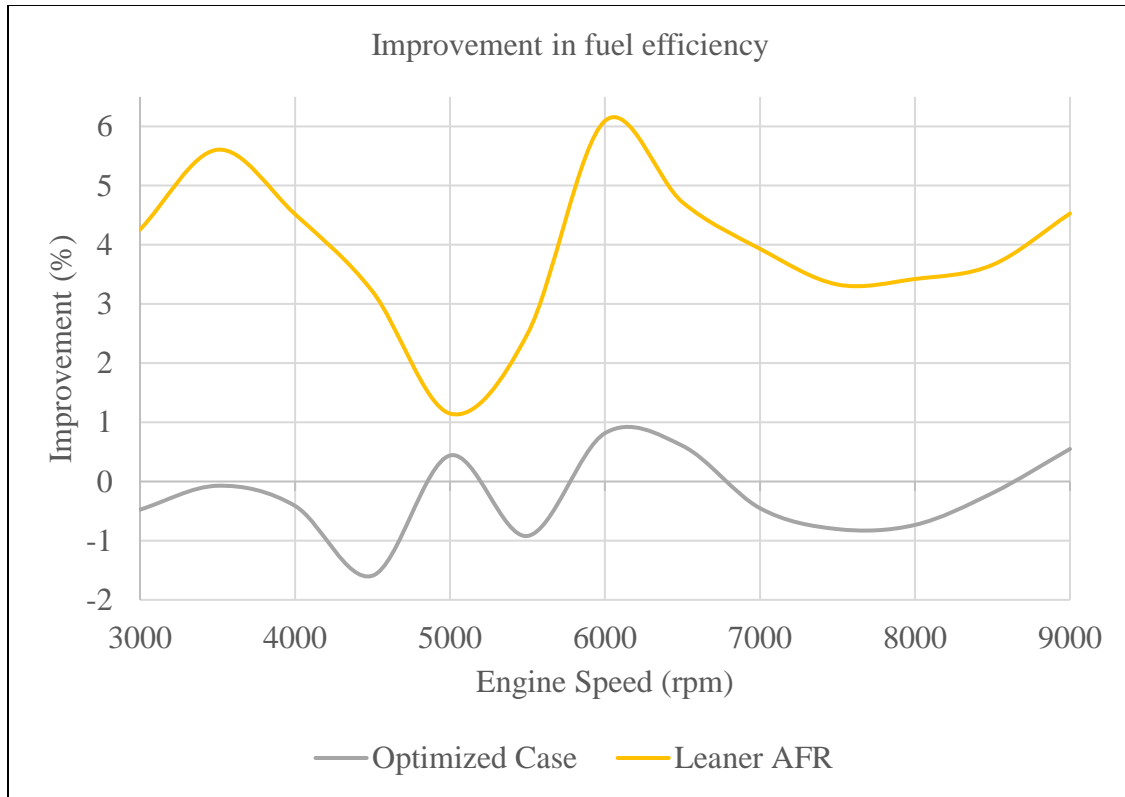


FIGURE 56: Percentage improvement in fuel efficiency

Figure 56 summarizes the improvements in fuel efficiency seen in Figure 54 and Figure 55. BSFC and thermal efficiency has reduced by 0.24 % on average because of the tuned variable induction manifold to optimize engine performance. When the air-fuel ratio is varied to bring down the power output to match the original performance, the fuel efficiency was considerably improved. It is improved by around 4.2 % on an average as compared to the engine with the optimized intake manifold. It is improved by 3.9 % as compared to the engines original performance and still produces the same power output as the engine originally did. A peak improvement of 6.1 % at 6000 rpm and the minimum improvement of 1.15 % is seen at 5000 rpm.

4: CONCLUSIONS

The effects of intake manifold tuning and intake valve tuning on the performance and fuel efficiency of an IC engine at WOT is successfully studied, simulated, observed, analyzed and presented using a commercially accepted 1-D simulation tool. It is observed that precise tuning can not only help, but also hurt the engine performance and efficiency. The uncertainty analysis of results obtained from this simulation tool shows that the simulation yields close to 98 % accurate results with combined standard uncertainty of ± 2.8 % with a coverage factor of 2. Hence, it can be said that this simulation tool is time and cost effective and yields fairly accurate results.

Engine volumetric efficiency is significantly improved due to the induction boost obtained by capitalizing the compression pressure waves in the intake manifold. These induction pressure waves are found to be very sensitive to the distance they travel in the intake manifold (intake runner length), the intake valve opening and closing time, and the area available for flow of air into the combustion chamber (valve lift). Intake runner length, intake valve timings and intake valve lifts, if varied individually over a large range with infinite variations can themselves optimize the engine performance. However, this is not feasible due to the manufacturing, assembly, space and cost constrains. To overcome these hurdles, the idea of varying them simultaneously has been suggested and the resulting effects on the performance and fuel efficiency have been simulated and analyzed. It is also observed that simultaneous variations not only reduce the span and number of the required variations, but also provide an extra boost to the volumetric efficiency, and thus the engine performance, by providing increased control on the induction pressure waves.

An appropriate selection of only two values (2-step variation) of the above mentioned parameters can also optimize the engine performance. An average improvement of 3.2 % in volumetric efficiency is encountered with the maximum improvement of 10.31 % at 3500 rpm and minimum improvement of 0 % at 8500 rpm when runner lengths are varied at all engine operating speeds. With the selection of intake runner length of 410 mm for 3000-6500 rpm speed range and 290 mm for 7000-9000 rpm speed range, the volumetric efficiency has boosted by an average of 1.4 %. But, this overall boost came at the cost of decrease in volumetric efficiency at a few engine speeds. To overcome these losses, valve opening timing are varied. When varied infinitely, an average improvement of 7.78 % is encountered in volumetric efficiency. This suggest that the co-existence of variations in runner lengths and valve timings can provide more boost to the volumetric efficiency as compared to boost provided by runner length variations in a small span alone. With the selection of intake valve opening time of 314 degree crank angle (CA) after top dead center (ATDC) for 3000-4500 rpm engine speed range and 338 degree crank angle (CA) after top dead center (ATDC) for 5000-9000 rpm engine speed range, the improvement in volumetric efficiency was limited to an average of 3.2 %. The losses in volumetric efficiency encountered at certain engine speeds after the selection of two runner lengths are recovered except at 5000 rpm, where a decrease of 1.21 % in volumetric efficiency is observed. To further boost the volumetric efficiency valve lifts are varied. When varied infinitely, the volumetric efficiency improved by 6.36 %. When valve lifts of 7.76 mm for 3000-5500 rpm range and 11.64 mm for 6000-9000 rpm range are selected, the volumetric efficiency improvement is found to be reduced to 6.22 %. Hence, it can be seen that major part of the decrease in the volumetric efficiency boost because to using

2-step variation instead of using infinite variations can be recovered by simultaneous 2-step variations of intake runner length, valve opening timing and valve lift.

It is observed that with the addition of variations in each parameter of the air induction system, the control on the induction pressure waves is increased. The occurrence of the high pressure wave is brought closer to the intake valve opening timing, thereby increasing the induction pressure. With the increase in induction pressure, an increase in the peak cycle pressure is encountered, thereby increasing the area under the P-V diagram and thus the engine power and torque output. Due to 2-step engine tuning, the power and torque output of the engine has increased by an average of 5.96 % with an average increase of 9.28 % at low revving speeds of 3000-5000 rpm, 4 % at mid-range revving speeds of 5000-7000 rpm and 3.87 % at high revving speeds of 7000-9000 rpm.

However, this increase in performance is accompanied by the decrease in thermal efficiency of the engine by 0.24 % thereby increasing the BSFC of the engine, making it less fuel efficient. To counter these losses, the engine can be run on leaner air-fuel mixtures. Hence the engine with the optimized induction assembly is run on variable air-fuel ratios to match the stock engine performance. It has been observed that running the engine of leaner air-fuel mixtures reduces the peak cycle pressure and temperature. The pumping work and the heat input to the system are still the same as they are for the optimized case. Hence, the thermal efficiency of the system is improved and the BSFC is reduced by an average of 3.9 % as compared to the stock engine.

It can be concluded from this research, that engine tuning using the method of 2-step variations can not only make engine tuning feasible, but can also be used for performance and fuel-efficiency enhancement as and when desired by the user.

5: REFERENCES

1. Heywood, J.B., Internal combustion engine fundamentals. Vol. 930. 1988: McGraw-hill New York.
2. Sawant, P. and S. Bari, Effects of Variable Intake Valve Timings and Valve Lift on the Performance and Fuel Efficiency of an Internal Combustion Engine. 2018, SAE International.
3. News, U. CAFE 2025 Available from: <https://www.usnews.com/news/articles/2012/08/29/545-miles-per-gallon-for-all-cars-by-2025-not-exactly>.
4. Moster, D.A., Intake Manifold Design for an Air Restricted Engine. 2012, University of Cincinnati.
5. Gokul, R. and R. Baliga, Continuously Variable Transmission.
6. Aradhye, O. and S. Bari, Continuously Varying Exhaust Pipe Length and Diameter to Improve the Performance of a Naturally Aspirated SI Engine. 2017(58417): p. V006T08A054.
7. Gajula, V. and S. Bari, Performance Tuning of an IC Engine Based on Pressure Wave Propagation With a Continuously Variable Exhaust Runner Length and Exhaust Valve Timing System. 2017(58417): p. V006T08A051.
8. Sawant, P. and S. Bari, Combined Effects of Variable Intake Manifold Length, Variable Valve Timing and Duration on the Performance of an Internal Combustion Engine. 2017(58417): p. V006T08A052.
9. Heywood, J., Internal combustion engine fundamentals. 1988: McGraw-Hill Education.

10. Khudhur, S.H., A.M. Saleh, and M.T. Chaichan, The Effect of Variable Valve Timing on SIE Performance and Emissions. *International Journal of Scientific & Engineering Research*, 2015. **6**(8): p. 173-179.
11. Kirkup, L. and R.B. Frenkel, *An introduction to uncertainty in measurement: using the GUM (guide to the expression of uncertainty in measurement)*. 2006: Cambridge University Press.
12. Malkhede, D.N. and H. Khalane, Maximizing Volumetric Efficiency of IC Engine through Intake Manifold Tuning. 2015, SAE Technical Paper.
13. Sammut, G. and A.C. Alkidas, Relative Contributions of Intake and Exhaust Tuning on SI Engine Breathing - A Computational Study. 2007, SAE International.
14. Vizard, D., *How to Super Tune and Modify Holley Carburetors*. Vol. 216. 2013: CarTech Inc.
15. Winterbone, D.E. and R.J. Pearson, *Design techniques for engine manifolds: wave action methods for IC engines*. 1999: Professional Engineering Publishing.
16. Bell, A.G., *Four-stroke performance tuning*. 1998: Cambridge University Press.
17. Hiraku, K., et al., Intake air amount control apparatus and method of internal combustion engine. 2004, Google Patents.
18. OH YIDE, A., *Design and Analysis of the Intake System of a Formula SAE Car*. 2012.
19. CHRYSLER 300 CLUB INTERNATIONAL, I.; Available from: <http://www.chrysler300club.com/uniq/allabouttrams/ramtheory.htm>.
20. Team. [cited Teamintegra.net; Available from: <http://www.team-integra.net/forum/blogs/michaeldelaney/130-intake-manifold-tech-runner-size->

[calculations.html](#).

21. Saravanan, D., A. Gokhale, and N. Karthikeyan, Design and Development of a Novel Charge Boosting System for a Single Cylinder SI Engine. 2014, SAE Technical Paper.
22. Fontana, G. and E. Galloni, Variable valve timing for fuel economy improvement in a small spark-ignition engine. Applied Energy, 2009. **86**(1): p. 96-105.
23. Stein, R., K. Galietti, and T. Leone, Dual equal vct-a variable camshaft timing strategy for improved fuel economy and emissions. 1995, SAE Technical Paper.
24. Integra, T. Intake Manifold Runner Calculations. Available from: <http://www.team-integra.net/forum/blogs/michaeldelaney/130-intake-manifold-tech-runner-size-calculations.html>.
25. International, C.C. Ram Air Theory. Available from: <http://www.chrysler300club.com/uniq/allaboutrams/ramtheory.htm>.
26. Gray, C., A review of variable engine valve timing. 1988, SAE Technical Paper.
27. Engine, I. Conventional Valve Timing Available from: <http://www.impulsenigne.com/how/valve.shtml>.
28. Khan, S.A. and P. Ayyappath, Design and development of variable valve timing and lift mechanism for improving the performance of single cylinder two wheeler gasoline engine. 2014, SAE Technical Paper.
29. Grutter, P.J., et al., Air induction control system for variable displacement internal combustion engine. 1995, Google Patents.
30. Cleary, D. and G. Silvas, Unthrottled engine operation with variable intake valve lift, duration, and timing. 2007, SAE Technical Paper.

31. Benedikt, K., et al., Further development of BMW's fully-variable valve control system valvetronic. MTZ worldwide, 2005. **66**(9): p. 10-13.
32. Baechtel, J., Practical Engine Airflow : Performance Theory and Application. 2015.
33. autozine.org. 3/7/2017]; Available from:
http://www.autozine.org/technical_school/engine/Intake_exhaust.html.
34. Hamilton, L.J., J. Cowart, and J. Rozich, The Effects of Intake Geometry on SI Engine Performance. 2009, SAE Technical Paper.
35. Thompson, M.P., Non-mechanical supercharging of a four-stroke diesel engine. 1968, The Ohio State University.
36. Racing, G.A. Induction Systems. Available from:
<http://grapeaperacing.weebly.com/uploads/4/1/2/0/41206275/inductionsystems.pdf>.
37. Engelman, H.W., Design of a tuned intake manifold. ASME paper, 1973(73-WA).
38. KTM. Owners Manual. Available from:
<http://www.ktmshop.se/documents/29660a4bab78e43834a5cd62155a8d05.pdf>.
39. Gilani, R., Engine Simulation Model for a Formula SAE Race Car. Applied Design, Development, Correlation and Optimization, 2012.
40. Software, R.; Available from: <https://www.software.ricardo.com/Products/WAVE>.
41. Liu, Y.C., A.J. Savas, and C.T. Avedisian, Comparison of the Burning Characteristics of Indolene and Commercial Grade Gasoline Droplets without Convection. Energy & Fuels, 2012. **26**(9): p. 5740-5749.
42. Ricardo. Wave Tutorials. Available from:
<https://www.software.ricardo.com/Products/WAVE>.

43. Sodré, J. and S. Soares, Comparison of engine power correction factors for varying atmospheric conditions. *Journal of the Brazilian Society of Mechanical Sciences and Engineering*, 2003. **25**(3): p. 279-284.